Determining human upper limb postures with an improved inverse kinematic method

by

Jiahuan Chen

A thesis submitted in partial fulfillment of the requirements for the degree of

Master of Science

Department of Mechanical Engineering
University of Alberta

Abstract

Body posture predicting methods have many applications, including product design, ergonomic workplace design, human body simulation, virtual reality and animation industry. Initiated in robotics, Inverse Kinematic (IK) method has been widely applied to proactive human body posture estimation. The Analytic Inverse Kinematic (AIK) method is a convenient and time-saving type of IK methods. It is also indicated that, based on AIK methods, a specific body posture can be determined by the optimization of an arbitrary objective function.

The objective of this thesis is to predict the postures of human arms during reaching tasks. In this research, a human body model is established in MATLAB, where the Middle Rotation Axis (MRA) analytic kinematic method is accomplished, based on this model. The joint displacement function and joint discomfort function are selected to be initially applied in this improved AIK method. Then a bi-criterion objective function is proposed by integrating the joint displacement function and joint discomfort function, with the suboptimal value of the coefficient, in the integrated objective function, determined by golden section search.

Results show that neither the joint displacement function nor the joint discomfort function predicts postures that are close enough to natural upper limb postures of human being, during reaching tasks. The accuracy of the arm postures, predicted by the proposed objective function, is the most satisfactory.

Preface

This thesis is an original work by Jiahuan Chen, under the supervision of Dr. Xinming Li. Chapter 1, chapter 2, chapter 4.1 and 4.2, as well as chapter 5.4 and part of chapter 6, have been published on *ROBOTICA* (Chen, J., & Li, X. (2022). Determining human upper limb postures with a developed inverse kinematic method. *Robotica,* 1-23. doi:10.1017/S0263574722000789), while Chapter 4.3, 4.4 and 4.5, as well as chapter 5.1, 5.2 and 5.3, have been published in a proceeding of the 2021 Canadian Society of Mechanical Engineering (CSME) conference (Chen, J. and Li, X., Development of a bi-criterion objective function for analytical inverse kinematic methods). The author also acknowledges that the experimental data, utilized for evaluating the performance of the improved inverse kinematic method (applied in the subsection 5.4), is extracted from the publication of Admiraal et al [1].

Acknowledgment

Jiahuan Chen would hereby highly appreciate the supervision and help from his supervisor, Dr. Xinming Li, during his Master's program, especially for guiding the case study, which intuitively exhibited the application of the developed methodology. Jiahuan also very appreciate Dr. Rouhani, for his lectures on Human Body Motion, where Jiahuan eventually got a relatively deep understanding of the motion sequences of rigid bodies, based on Euler-Cardan angles, which later became a basis of the research shown in this thesis.

When it comes to the financial support, Jiahuan would sincerely acknowledge that this research is funded by the Natural Sciences and Engineering Research Council of Canada (NSERC) through the supervisor's Discovery Grant (RGPIN-2019-04585), where he got essential help to pay for his tuition fees and living expenses. He would also highly appreciate the Department of Mechanical Engineering, for choosing him to receive the Graduation Completion Scholarship. Last but not the least, he would also like to say "thank-you" to his parents, Mrs. Li and Mr. Chen, for funding the last year of his Master's program. Without all the help mentioned above, he would never have the chance to finish his Master's project and get a degree.

Table of Contents

List of Tables

List of Figures

List of Symbols

(In the order of logic; Emboldened symbols indicate vectors or matrices, while common symbols indicate scalars.)

1. Kinematic Structure

   $\mathbf{X_i}$ – the position vector of the i^{th} joint (or anatomical landmark)

   $\mathbf{V_i}$ – the vector which represents the length and orientation of the i^{th} body segment, named as segmental vector

   $\mathbf{V_i^{(0)}}$ – the segmental vector of the i^{th} body segment, in the neutral standing posture.

   α_{ij} – the j^{th} joint angle of the i^{th} joint.

   $\boldsymbol{\alpha}$ – the matrix made up with all the joint angles (α_{ij}), named as joint angle matrix.

   $\mathbf{R_i}$ – the rotation matrix of the i^{th} joint, described in **section 3.2**.

2. Analytic Inverse Kinematic Method

   ϕ – swivel angle, described in **section 2.1**.

   τ – shoulder twist, the same angle as the shoulder rotation angle ($\alpha_{6,4}$).

   $\mathbf{d_t}$ – the vector pointing from the right shoulder joint centre ($\mathbf{X_6}$) to the target point position **T**

   $\mathbf{d_t'}$ – the vector pointing from the right shoulder joint centre ($\mathbf{X_6}$) to the 2^{nd} right fingertip ($\mathbf{X_8}$).

3. Body Posture Optimization

   a. Shoulder joint limit model

      $\mathbf{e_{sx}}$, $\mathbf{e_{sy}}$, $\mathbf{e_{sz}}$ – element vectors of the shoulder joint coordinate system (in different directions from the global coordinate system).

$\mathbf{e_{jx}}$, $\mathbf{e_{jy}}$, $\mathbf{e_{jz}}$ – element vectors of the shoulder joint limit coordinate system.

$X_jY_jZ_j$ – shoulder joint limit coordinate system.

ϕ_n, θ_n – orientation angles used for determining the orientation of $\mathbf{e_{jz}}$ (which is also the neutral orientation of the right upper arm).

S_s – the swing angle of the right shoulder joint.

d – a vector in the direction of the right upper arm, with a scale equal to S_s.

S_x, S_y – x and y components of S_s.

r_x, r_y – limitation values of S_x and S_y.

b. Objective functions

f_{dpe} – Delta Potential Energy function;

$f_{discomf}$ – the joint discomfort function;

$f_{displace}$ – the joint displacement function;

f_{obj} – an arbitrary objective function, which can be f_{dpe}, $f_{discomf}$, $f_{displace}$, etc., or any other objective function to be proposed by future researchers.

4. Proposed bi-criterion objective function

$f_{discomf\text{-}displace}$ – the proposed bi-criterion objective function, which combines the joint discomfort function and the joint displacement function;

α – coefficient of the joint discomfort function ($f_{discomf}$) in the proposed bi-criterion objective function ($f_{discomf\text{-}displace}$).

a. Search the suboptimal value of α

R^2 – coefficient of determination, defined as the subtraction of the Sum of Squares of Residuals (SSR), divided by the Total Sum of the Squares (TSS) of linear regression values, from one;

α_{opt} – the suboptimal value of α.

b. Residual analysis

$\zeta_{residual}$ – residual of the shoulder rotation angle (unit: degree), defined as the difference between the measured shoulder rotation value ($\zeta_{measured}$) and the regression value of the shoulder rotation angle ($\zeta_{regression}$). (To summarize, in this thesis, all the symbols $\alpha_{6,4}$ (for the kinematic structure), τ (for the analytical inverse kinematic method) and ζ refer to the right shoulder rotation angle. The author hereby sincerely apologize for the inconvenience to readers.)

Glossary of Frequently-Appeared Terms (Abbreviations)

(In the order of logic)

1. Kinematic Structure

   Kinematic Structure: the geometry of the studied part of human body.

   Motion Equations: equations that describe the connections among joint angle values, segmental vector orientations and joint (or anatomical landmark) positions.

   Human body modeling: the sum of Kinematic Structure and Motion Equations.

2. Analytic Inverse Kinematic Method

   Inverse Kinematic (IK) problem: The problem of determining appropriate body postures (i.e. appropriate configurations of joint-angle values) to reach a desired position (i.e. target position) for the end-effector.

   Inverse Kinematic (IK) method: the method used to solve the inverse kinematic problem.

   Analytic Inverse Kinematic (AIK) method: IK methods which are developed to find out the solution as a function of the target point position.

3. Body Posture Optimization

   Body Posture Optimization (BPO): An optimizational way to determine body postures (i.e. Determine body postures by modeling the determination as an optimization problem. In this thesis, BPO is the same concept as numerical IK methods.)

Shoulder joint limit model: The sum of the shoulder joint limit coordinate system (marked as "$X_jY_jZ_j$" in this thesis) and the equation which describes the possible range of the upper arm.

Chapter 1 Introduction

Proactive body posture estimation is very important to a wide spectrum of areas, ranging from product design to ergonomic simulation. To be specific, first, it can be applied in virtual design of workspace [2][3][4]; an example is that it has been validated in the proactive determination of human body postures while reaching buttons in a car, which can help to re-design the location of those buttons [3]. Secondly, it is useful for the ergonomic simulation of manual tasks [5][6][7][8][9]. With proactively estimated body postures, the corresponding ergonomic risks will be proactively assessed, and necessary adjustments will be proactively made to the task [6][7]; It is also useful for virtual reality and computer graphics. In virtual reality, it can be applied to improve the embodiment of human characters [10]; while in computer graphics, it can be utilized to generate the animation of human models or the models of other legged creatures [11].

1.1 Inverse kinematic methods for robotics

The problem of proactively determining appropriate body postures (i.e. appropriate configurations of joint-angle values), based on a desired target point position, is named as Inverse Kinematic (IK) problem [11] (A schematic of the IK problem is given in **Figure 1**), which was initiated in robotics, in order to move the end-effector of a robotic manipulator to desired positions [11][12]. Before the appearance of inverse kinematic solutions, robotic manipulator control is mainly based on master-slave systems [13], which require the operation from human workers [12]. Denavit and Hartenberg developed a four-by-four matrix to formulate the kinematics of linkage systems [14], which was later used to analyze the motion of four-link systems [15]. The same

concepts and similar method were later applied to the human upper limb [16], which is regarded as a seven-link system.

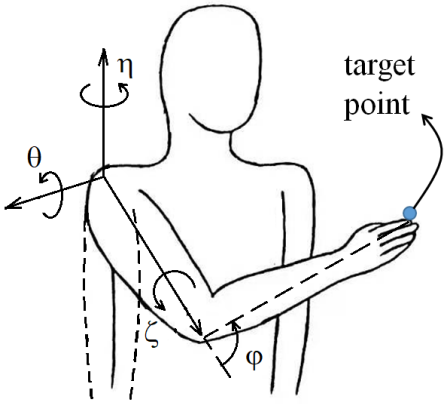

Figure 1 Schematics of the inverse kinematic problem of human upper limb. (Dashed line shows the initial position of the arm. η, θ, ζ, φ are the joint angles, which are the shoulder adduction, shoulder flexion, shoulder rotation and elbow flexion, respectively.)

1.2 Inverse kinematic methods for human motion and contributions of this thesis

In the control of robotic manipulators, inverse kinematic solutions avoid the inconvenience and excessive time delay [12]. Apart from its application on robotics, IK methods have later been widely applied for analysis of human motion. This research focuses on analytic IK methods, which is a convenient and time-saving sort of IK methods, and has already been widely applied to the analysis of human motion [16][18][19]. In this research, an optimization module is merged into a previous analytic IK method, in order to increase the accuracy of the previous methods. In the optimization module, two objective functions (the joint displacement function and the joint discomfort function) are combined to form a bi-criterion objective function. The coefficient value

of the joint discomfort part, in this bi-criterion objective function, is then determined, based on experimental data of a reaching task extracted from the publication of other researchers [1].

1.3 Analytic Inverse Kinematic (AIK) method

IK methods can be categorized into three major types. One of them is the data-driven IK methods, which use pre-learned postures to match the given positions of the end-effectors [11]. Another type of IK methods is the numerical IK methods [10]. Numerical IK methods achieve satisfactory solutions through a set of iterations, without considering the mechanism of the studied kinematic structure. In the numerical IK methods, an object for the iterations will be initially set. Then, different sets of joint angle values will be attempted, in order to minimize/maximize the value of the object, while each joint angle is mathematically treated as equivalent.

Analytic Inverse Kinematic (AIK) methods are reliable IK methods which usually do not have singularity problems [11]. They are meant to find out the solution as a function of the target point position. For example, as shown in **subsection 4.1**, the elbow flexion angle is directly formulated as a function of distance between the target position and the shoulder position. Compared with analytic IK methods, numerical IK methods can achieve better accuracy, but require 400-600 times of the time that analytic IK methods usually need [17]. When it comes to data-driven IK methods, they ensure natural body-postures, but need a large amount of motion data for each task, which is expensive and time-consuming to acquire [10] [11]. Therefore, this research focuses on Analytic Inverse Kinematic (AIK) methods.

1.4 Swivel Angle and Research Objectives

For upper-limb applications, elbow flexion is initially solved in AIK methods, based on the target distance from wrist joint centre to shoulder joint centre. Then, the elbow joint position is limited on a circle shown in **Figure 2**. In order to parameterize the elbow position, the swivel angle ϕ is defined to evaluate the rotation of arm (shown in **Figure 2**) [16][18][19], which is defined around the middle rotation axis (an axis pointing from shoulder joint centre to wrist joint centre)

The swivel angle can be limited by means of applying joint limit models [18][19]. However, joint limits can only provide a possible range of angles, instead of a specific swivel angle [11]. Therefore, the first objective of this thesis is to seek a scientific approach to exactly determine the swivel angle, thus to exactly determine the upper limb posture.

Tolani et al pointed out three ways of selecting an appropriate swivel angle, from the possible range of angles: (1) select the midpoint of the possible range; (2) choose a possible value which is closest to a desired value; (3) find a swivel angle value of ϕ which minimizes an arbitrary objective function [16]. This research focuses on the third approach, combining objective functions with the analytic IK method, in order to find an accurate solution. Therefore, the second objective is to find an appropriate function for the improved IK method. In addition, through the seek for an appropriate objective function, the third objective of this thesis is to explore the mechanisms of the body posture determination.

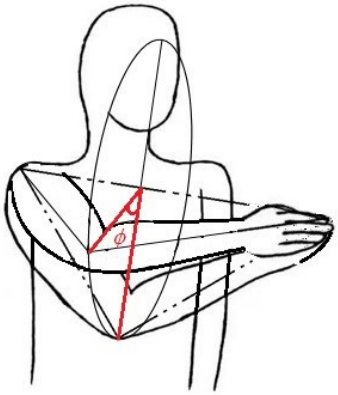

Figure 2 Swivel angle ϕ.

1.5 Outlines

In general, the contents of this thesis are separated into six chapters, where this **first chapter** introduces the background of this research. Then, the **second chapter** provides a view of the Body Posture Optimization (BPO) method, as well as an accordance of the selection of the objective function, used in the BPO module of the improved method.

The **third chapter** is a description of the established human body model, which is the foundation of the implementation of the improved AIK method. The **fourth chapter** is a description of my methodology, which initially introduced how I implement the previous AIK method, in the established human body model, followed by a description of the combination between the previous AIK method and the BPO method. Finally, **Chapter 5** and **Chapter 6** shows the results and conclusions, respectively.

Chapter 2 Literature review

This chapter provides a deeper view of the research background. **Section 2.1** exhibits the formulation of the Body Posture Optimization (BPO) method, where the objective function is a vital component. A literature review (shown in **Table 1**) is then conducted to determine which cost function(s) to be applied in the improved IK method. Among reviewed publications, the joint discomfort function, joint displacement function and the delta potential energy function are top-three of the most commonly-applied cost functions, whose physical meanings and feasibilities are thus introduced in **section 2.2**, **2.3** and **2.4**.

2.1 Body Posture Optimization and Cost Function

In this thesis, Body Posture Optimization (BPO) is combined into a previous AIK method, in order to achieve a scientific determination of the swivel angle. Previous body posture optimization problem is defined as follows. Previous researchers try to find the configuration (joint angles **q**) of a human body when the fingertip or other end-effector reaches the target point [3]. The hypothesis is that human performance measures govern the movements of human bodies. Based on this hypothesis, the BPO problem can be formulated as follows [3][20][21]:

Find: $\boldsymbol{q} \in R^{DOF}$

to minimize: $f_{obj}(\boldsymbol{q})$

subject to: $distance = \| \boldsymbol{x}_{end\text{-}effector}(\boldsymbol{q}) - \boldsymbol{x}_{target\text{-}point} \| < \varepsilon$

$q_i^L < q_i < q_i^U$ ($i = 1, 2, \ldots, DOF$)

where f_{obj} is an arbitrary objective function;

q is the joint angle vector, whose elements are joint vectors;

R indicates the real number space;

ε is a small number close to zero;

$\mathbf{x}_{\text{end-effector}}(\mathbf{q})$ is the position vector of the end-effector, as a function of the joint angles;

$\mathbf{x}_{\text{target-point}}$ is the position vector of the target point;

DOF is the total number of the degree-of-freedom of the applied kinematic structure.

q_i is the i^{th} element of the joint angle vector **q**, which is equal to the i^{th} joint angle of the kinematic structure;

q_i^L and q_i^U are the lower and upper limits of the i^{th} joint angle, respectively.

Cost functions are functions evaluating human performance measures [20], which can be applied as the objective functions, for the determination of human body posture. One thing that the authors wish to point out here is that this thesis combines AIK with the body posture optimization method, where the joint limit model of AIK performs as the constraint (details are discussed in the methodology section). Therefore, this section discusses different objective functions without considering the complete constrained optimization problem.

In order to determine which cost function(s) to be applied in this research, a literature review has been conducted (shown in **Table 1**). Thirteen publications are studied in this review (**Table 1**). Since one of the aims of this research is studying the mechanism of body-posture prediction, only those publications, related to human postures, are studied, while publications on robotics are

excluded. Among selected publications, the joint discomfort function is the most commonly-applied cost function. The joint displacement function and delta potential energy function are the second most commonly-applied cost functions. Therefore, the joint discomfort function, joint displacement function and delta potential energy function are analyzed in this research.

It is also exhibited that, based on searched literature, previous objective functions can be categorized into single objective functions and multiple objective functions. (In this section, bi-criterion objective functions are also categorized as multiple objective functions.) Multiple objective functions can also be categorized into two types: one is the product of different cost functions [22], while the other is weighted sum of different cost functions [2][9][3]. It has been reported that the combination of different cost functions (i.e. multiple objective functions [23]) is able to increase the accuracy of predicted body postures [1]. However, based on searched literature, there is not a systematic approach to accurately determine the weights of different cost functions [24]. In addition, previous research has not clarified how the different cost functions coupled together are.

Table 1 Selected studies and applied cost functions for the literature review

No.	Year	Title of publication	Applied cost functions
1	1994	Psychophysical cost function of joint movement for arm reach posture prediction [25]	- joint discomfort
2	1995	Inverse Kinetics for Center of Mass Position Control and Posture Optimization [34]	- support torque (from the ground) - joint effort
3	1996	Optimal posture of a human operator and CAD in robotics [35] (via [2])	- joint torque
4	2009	Use of multi-objective optimization for digital human posture prediction [2]	- joint displacement - joint discomfort - delta potential energy
5	2009	Optimization-based posture prediction for human upper body [20]	- joint displacement
6	2011	Multi-objective optimization-based method for kinematic posture prediction: development and validation [3]	- joint discomfort - delta potential energy
7	2011	Optimization-based posture prediction for analysis of box lifting tasks [8]	- Joint torque
8	2012	A Bi-Criterion Model for Human Arm Posture Prediction [23]	- joint displacement
9	2012	An inverse optimization approach for determining weights of joint displacement objective function for upper body kinematic posture prediction [26]	- joint displacement
10	2013	A New Criterion for Redundancy Resolution of Human Arm in Reaching Tasks [24]	- gravitational potential energy - elastic potential energy
11	2018	Optimization of Posture Analysis in Manual Assembly [36]	- joint discomfort - total energy expenditure
12	2020	Optimization of Posture Prediction Using MOO in Brick Stacking Operation [22]	- joint discomfort - total energy expenditure
13	2020	Multi-Objective Optimization Method for Posture Prediction of Symmetric Static Lifting Using a Three-Dimensional Human Model [9])	- joint torque - delta potential energy - compression/tension forces - shear forces (vertebrate) - joint discomfort - sight angle (eyesight)

2.2 Delta potential energy

Delta potential energy describes the change of the gravity potential energy of human body, from initial posture to final posture [20]. Equation (1) shows a commonly-applied formulation of the delta potential energy function [20].

$$f_{dpe}(\boldsymbol{q}) = \sum_{i=1}^{n}(m_i \cdot g)^2 \cdot (\Delta h_i)^2 \quad (1)$$

where, m_i is the mass of the i_{th} body segment (Usually, a unit of kilogram is applied. In this research, m_i is normalized by the body mass. Therefore, body mass is applied as the unit.),

g is the gravitational acceleration (The body mass multiplied by the gravitational acceleration is body weight. Therefore, the body weight (BW) is applied as the unit of $m_i g$.),

Δh_i is the change of the height, of the centre of mass of the i_{th} body segment, from the initial body posture to the final body posture (unit: meter or millimeter; millimeter is applied in this research).

For each couple of initial target point and final target point, as the swivel angle increases, Δh_i will also increase, so that the delta potential energy of human arm will keep increasing. Therefore, the pure minimization of delta potential energy will always lead to the smallest swivel angle, which is probably not an accurate optimization.

2.3 Joint discomfort

The joint discomfort function has been widely applied to predict body-posture [25][20][22], which evaluates the musculoskeletal discomfort of human body [2]. Based on searched literature, the latest joint discomfort function is developed by Marler et al [21] (shown in equation (2)).

$$f_{discomf}(\boldsymbol{q}) = \frac{1}{G} \cdot \sum_{i=1}^{n} [\gamma_i \cdot (\Delta q_i^{n,norm}) + G \cdot QU_i + G \cdot QL_i] \tag{2}$$

$$\Delta q_i^{n,norm} = \frac{q_i - q_i^n}{q_i^u - q_i^L} \tag{3}$$

$$QU_i = (0.5 \cdot sin(\frac{5.0 \cdot (q_i^U - q_i)}{q_i^U - q_i^L} + 1.571) + 1)^{100} \tag{4}$$

$$QL_i = (0.5 \cdot sin(\frac{5.0 \cdot (q_i - q_i^L)}{q_i^U - q_i^L} + 1.571) + 1)^{100} \tag{5}$$

where, q_i is the value of i_{th} joint angle (unit: degree or rad),

q_i^n is the neutral value of i_{th} joint angle (unit: degree or rad),

(It is discovered that the neutral direction of the upper arm is corresponding to the minimum discomfort status of the shoulder joint. In this thesis, the neutral values of shoulder joint angles are cited from the research of Engin and Chen, where ten subjects are involved in their experiment. [30])

q_i^U is the upper limit of the i_{th} joint angle (unit: degree or rad),

q_i^L is the lower limit of the i_{th} joint angle (unit: degree or rad),

$\Delta q_i^{n,norm}$ is the normalized value of the i_{th} joint angle, based on the neutral joint angle value (as shown in equation (3)). Therefore, it has no unit.

γ_i is the joint weight (without unit),

QU_i is the joint limit term expressed in equation (4),

QL_i is the joint limit term expressed in equation (5),

G is a magnifying ratio (G > 1) for the joint limit terms QU_i and QL_i. The function in equation (2) is divided by G, in order to prevent the joint discomfort function from having extremely high values, when compared with the other cost functions. [2].

For each joint, they evaluate its discomfort by two facts: (a) joint discomfort decreases when a segment get close to its neutral position; (b) joint discomfort rapidly increases when a segment get close to its limits [2]. Based on searched literature, its performance has not been evaluated by experiment data. Therefore, in this research, the performance of the joint discomfort function is evaluated by extracted experiment data, before being combined with another cost function.

2.4 Joint displacement

The joint displacement evaluates the angular displacement of each joint. In some research, the joint displacement is calculated from the neutral position [20][2], while, in other research, it is calculated from the initial position (i.e. the starting posture of the current analyzed motion or the end posture of a previous motion if a continuous motion is analyzed) [23]. When calculated from the initial position, the joint displacement is proportional to the energy expenditure of the motion from initial posture to final posture [23], which estimates the effect of the initial posture to the final posture. Therefore, in this research, joint displacement is calculated from initial posture. A commonly-used formulation of the joint displacement function is shown in equation (6) [26].

$$f_{displace}(\boldsymbol{q}) = \sum_{i=1}^{n} \omega_i \cdot \left(\Delta q_i^{i,norm}\right)^2 \tag{6}$$

$$\Delta q_i^{i,norm} = \frac{q_i - q_i^i}{q_i^u - q_i^L} \tag{7}$$

where, q_i^i is the initial value of i_{th} joint angle (unit: degree or rad),

ω_i is the joint weight of the i_{th} joint angle (with no unit).

$\Delta q_i^{i,norm}$ is the normalized value of the i_{th} joint angle, based on the initial joint angle value (shown in equation (7) [2]). Therefore, it has no unit.

Zou et al determined the weights in joint displacement function by means of inverse optimization [26]. Their joint displacement function is validated in whole-body reaching tasks and predicts reasonably accurate body postures [26]. However, when the torso is fixed, the accuracy of the determined joint angle values turns out to be low, which exhibits that the joint displacement function is not feasible for all types of reaching tasks. Further analysis needs to be conducted on its performance.

Therefore, in this research, Simulations focus on the reaching tasks without motion of torso. Selected single objective functions (the joint displacement function and joint discomfort function) were initially combined with AIK method, respectively, and then this research examined the accuracy of the body postures, predicted by the joint displacement function [26] and the joint discomfort function [21]. Next, the selected single objective functions were comprehensively combined, proposing a new bi-criterion objective function. Furthermore, this research has also validated the accuracy of the improved AIK method, with this proposed bi-criterion objective function, and studied the effect of the weight of joint discomfort, on the accuracy of the determined joint angle values.

Chapter 3 Kinematic models

In order to combine the AIK method with an optimization model (i.e. adding objective functions to the AIK method), a rigid-segmental human body model [14] is established in Matlab, according to the body segment parameters exhibited in a publication of Dumas et al [27].

3.1 Segmental vectors

This model consists of vectors and nodes (**Figure 3.1 (a) and (b)**). The torso segment is modelled by three vectors (**V_4, V_5, V_{11}**), while the pelvis segment is modelled by two vectors (**V_3, V_8**). The other segments are all modelled as single vectors. The origin is located at the right heel **X_1**. Although the proposed IK method is based on this rigid-segmental human body model, this model is independent from the IK method and is possible to have other application. In addition, although the currently proposed IK method focuses on the determination of upper limb posture, this IK method can be expanded to the entire body in the future. Therefore, all the body segments have been included in this model.

$$i = 1, \quad \boldsymbol{X_i} = \boldsymbol{O_b} \tag{8.1}$$

$$i = 0 \sim 5, \quad \boldsymbol{X_i} = \boldsymbol{O_b} + \sum_{j=1}^{i-1}(-\boldsymbol{V_j}) \tag{8.2}$$

$$i = 6, 7, 8, \quad \boldsymbol{X_i} = \boldsymbol{O_b} + \sum_{j=1}^{4}(-\boldsymbol{V_j}) + \sum_{j=5}^{i-1}\boldsymbol{V_j} \tag{8.3}$$

$$i = 9, 10, 11, \quad \boldsymbol{X_i} = \boldsymbol{O_b} + \sum_{j=1}^{3}(-\boldsymbol{V_j}) + \sum_{j=8}^{i-1}\boldsymbol{V_j} \tag{8.4}$$

$$i = 12, 13, 14, \quad \boldsymbol{X_i} = \boldsymbol{O_b} + \sum_{j=1}^{4}(-\boldsymbol{V_j}) + \sum_{j=11}^{i-1}\boldsymbol{V_j} \tag{8.5}$$

$$i = 15, \quad \boldsymbol{X_i} = \boldsymbol{O_b} + \sum_{j=1}^{4}(-\boldsymbol{V_j}) + \boldsymbol{V_{14}} \tag{8.6}$$

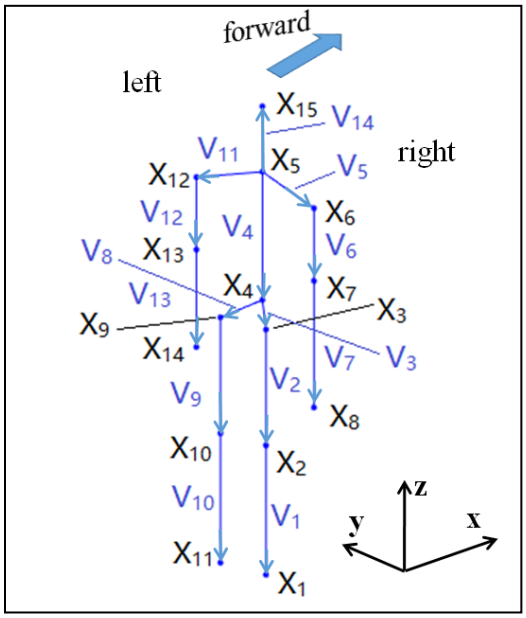

(a)

Node number	Corresponding joint / anatomical landmark
1	Right heel
2	Right knee
3	Right hip
4	Waist
5	Neck
6	Right shoulder
7	Right elbow
8	Right 2nd fingertip
9	Left hip
10	Left knee
11	Left heel
12	Left shoulder
13	Left elbow
14	Left 2nd fingertip
15	top of head

(b)

Figure 3. 1 Kinematic structure of the established human body model. (a) Back view of the established human body model; (b) Anatomical meaning of body nodes.

3.2 Joint angles

Segmental vectors are motivated by joint angles. In this model, the reference of the rotation of each segment is based on the orientation of the pelvis. Then, the rotation of the pelvis segment, relative to the global coordinate system, is defined by the three Euler rotation angles, which is described in subsection 3.2.1.

3.2.1 General definitions

Generally speaking, each joint ($\mathbf{X_i}$) has an index i, as illustrated in **Figure 3.1 (a)**. For example, the joint index for the right shoulder joint is 6 (**Figure 3.1 (b)**). For an arbitrary joint with a joint index i, joint angles are defined by global-frame-based ZYZ Sequence. To be specific, the rotation of each joint is divided into three rotations. In the first rotation, an angle $\alpha_{i,4}$ is performed around the z-axis, where i is the joint index. In the second rotation, an angle $\alpha_{i,2}$ is performed around the y-axis of the global coordinate system. Finally, in the third rotation, an angle $\alpha_{i,3}$ is performed around the z-axis of the global coordinate system again. Thus, the rotation matrix of an arbitrary joint i ($\mathbf{R_i}$) can be deduced as equation (9.1), which is equivalent to Euler's ZYZ Sequence.

$$\boldsymbol{R_i} = \boldsymbol{R_z}(\alpha_{i,3}) \cdot \boldsymbol{R_y}(\alpha_{i,2}) \cdot \boldsymbol{R_z}(\alpha_{i,4}) \tag{9.1}$$

Where $\mathbf{R_y}$ and $\mathbf{R_z}$ represent basic rotation matrices, around y and z axes, respectively.

The basic rotation matrices around y and z axes, with an arbitrary rotational angle α, $\mathbf{R_y}(\alpha)$ and $\mathbf{R_z}(\alpha)$, can be calculated as equation (9.2) and (9.3).

$$\boldsymbol{R_y}(\alpha) = \begin{pmatrix} \cos\alpha & 0 & \sin\alpha \\ 0 & 1 & 0 \\ -\sin\alpha & 0 & \cos\alpha \end{pmatrix} \tag{9.2}$$

$$\boldsymbol{R}_z(\alpha) = \begin{pmatrix} \cos\alpha & -\sin\alpha & 0 \\ \sin\alpha & \cos\alpha & 0 \\ 0 & 0 & 1 \end{pmatrix} \tag{9.3}$$

Based on this adjusted notation for joint angles, an adjustment has also been made to the storage of the joint angles. In previous research, all the joint angles are stored as a vector, which can make it difficult for users to match the index of a joint angle with its anatomical meaning. As **Figure 3.2** shows, in this research, all the joint angles are stored in a matrix, where the first index is the joint notation, and the second index is the axis notation. In order to make the index easy to remember, the axis indices 1, 2 and 3 are matched with the x, y and z axes of the global coordinate system, respectively. Since there are two rotational angles around the z axis, the first rotational angle $\alpha_{i,4}$ is stored in the fourth column.

In order to make all the definitions above more intuitive, a plot of the kinematic structure of the right upper limb (**Figure 3.3**), applied in this thesis, is attached to subsection 3.2.4.

$$\alpha = \begin{pmatrix} 0 & \alpha_{1,2} & \alpha_{1,3} & \alpha_{1,4} \\ 0 & \alpha_{2,2} & 0 & 0 \\ 0 & \alpha_{3,2} & \alpha_{3,3} & \alpha_{3,4} \\ 0 & \alpha_{4,2} & \alpha_{4,3} & \alpha_{4,4} \\ 0 & \alpha_{5,2} & \alpha_{5,3} & \alpha_{5,4} \\ 0 & \alpha_{6,2} & \alpha_{6,3} & \alpha_{6,4} \\ 0 & \alpha_{7,2} & 0 & 0 \\ 0 & 0 & 0 & 0 \\ 0 & \alpha_{9,2} & \alpha_{9,3} & \alpha_{9,4} \\ 0 & \alpha_{10,2} & 0 & 0 \\ 0 & \alpha_{11,2} & \alpha_{11,3} & \alpha_{11,4} \\ 0 & \alpha_{12,2} & \alpha_{12,3} & \alpha_{12,4} \\ 0 & \alpha_{13,2} & 0 & 0 \\ 0 & 0 & 0 & 0 \\ 0 & 0 & 0 & 0 \end{pmatrix}$$

Figure 3. 2 Joint angle matrix of the entire body modeling.

3.2.2 Movements of the pelvis

In this model (as shown in **Figure 3.1**), the pelvis segment is modelled by two vectors, $\mathbf{V_3}$ and $\mathbf{V_8}$, which point from the waist joint center ($\mathbf{X_4}$) to the right hip joint center ($\mathbf{X_3}$) and the left hip joint center ($\mathbf{X_9}$), respectively. Then, the orientation of the pelvis segment is able to be defined by the Euler rotation angles, in respect to the global coordinate system.

Similar to the joint angles, the orientation angles of the pelvis segment, defined in this thesis, also obey the ZYZ Euler sequence (described in subsection 3.2.1). The only difference is that there is not a joint index for the pelvis segment, in the joint angle matrix. Therefore, another angle vector, named as $\mathbf{a_p}$, is created to store the pelvis orientation angles (shown in equation 10.1). In this way, the pelvis orientation angles, a_{p2}, a_{p3} and a_{p4}, represent the pitch, yaw and roll of the pelvis segment, respectively; while readers may imagine a 'virtual joint' between the pelvis segment and the global coordinate system, in order to have a better understanding on the pelvis orientation angles.

$$\boldsymbol{\alpha_p} = (0, \alpha_{p2}, \alpha_{p3}, \alpha_{p4}) \tag{10.1}$$

Therefore, the rotation matrix of the pelvis segment ($\mathbf{R_p}$) is formulated as equation (10.2), where the symbols R_y and R_z apply the same meaning as displayed in subsection 3.2.1. Then the pelvis segmental vectors, $\mathbf{V_3}$ and $\mathbf{V_8}$, are able to be calculated by equation (10.3) and (10.4).

$$\boldsymbol{R_p} = \boldsymbol{R_z}(\alpha_{p4})\ \boldsymbol{R_y}(\alpha_{p2})\ \boldsymbol{R_z}(\alpha_{p3}) \tag{10.2}$$

$$\boldsymbol{V_3} = \boldsymbol{R_p}\ \boldsymbol{V_3^{(0)}} \tag{10.3}$$

$$\boldsymbol{V_8} = \boldsymbol{R_p}\ \boldsymbol{V_8^{(0)}} \tag{10.4}$$

3.2.3 Movements of the torso and head

As shown in Figure 3.1, the torso segment is modelled by three vectors, $\mathbf{V_4}$, $\mathbf{V_5}$ and $\mathbf{V_{11}}$, which represent the spine, the right clavicle and the left clavicle, respectively. In this model, the movements of the left clavicle and the right clavicle, in respect to the spine, are not involved, since the main aims of the establishment of this human body modeling is to provide a foundation for the development of an improved IK method (for the determination of upper-limb postures in a specific type of reaching tasks), as well as to validate the feasibility of building a whole-body model in a universal mathematical software (e.g. MATLAB). For the same targets, the deformation of the entire spine is represented by the bending of the waist joint.

In this way, the joint angle $\alpha_{4,2}$ represents the bending of the spine, while the other two waist joint angles, $\alpha_{4,3}$ and $\alpha_{4,4}$, themselves, do not have specific physical meaning. However, the other two waist joint angles, $\alpha_{4,3}$ and $\alpha_{4,4}$, will assist the joint angle $\alpha_{4,2}$ in representing those torso movements other than the bending. For example, if $\alpha_{4,3} = \alpha_{4,4} = 90$ degree, the value of $\alpha_{4,2}$ would indicate the abduction angle of the waist joint.

Therefore, according to the general definitions of joint angles and joint rotation matrices (described in subsection 3.2.1) in this thesis, the rotation matrix of the waist joint ($\mathbf{R_4}$) is formulated as equation (10.5), where the symbols R_y and R_z apply the same meaning as displayed in subsection 3.2.1. Then the torso segmental vectors, $\mathbf{V_4}$, $\mathbf{V_5}$ and $\mathbf{V_{11}}$, are able to be calculated by equation (10.6) (10.7) and (10.8).

$$\boldsymbol{R_4} = \boldsymbol{R}_z(\alpha_{4,4})\ \boldsymbol{R}_y(\alpha_{4,2})\ \boldsymbol{R}_z(\alpha_{4,3}) \tag{10.5}$$

$$\boldsymbol{V_4} = \boldsymbol{R_p}\,\boldsymbol{R_4}\,\boldsymbol{V_4^{(0)}} \tag{10.6}$$

$$\boldsymbol{V_5} = \boldsymbol{R_p}\,\boldsymbol{R_4}\,\boldsymbol{V_5^{(0)}} \tag{10.7}$$

$$\boldsymbol{V_{11}} = \boldsymbol{R_p}\,\boldsymbol{R_4}\,\boldsymbol{V_{11}^{(0)}} \tag{10.8}$$

Then, for the movements of the head segment, neck joint angles $\alpha_{5,2}$, $\alpha_{5,3}$ and $\alpha_{5,4}$ represents the flexion/extension, abduction/adduction and rotation of the neck joint, respectively. Therefore, the rotation matrix of the neck joint ($\mathbf{R_5}$) is expressed as equation (10.9). Then the head segmental vector, $\mathbf{V_{14}}$, is able to be calculated by equation (10.10).

$$\boldsymbol{R_5} = \boldsymbol{R_z}(\alpha_{5,4})\ \boldsymbol{R_y}(\alpha_{5,2})\ \boldsymbol{R_z}(\alpha_{5,3}) \tag{10.9}$$

$$\boldsymbol{V_{14}} = \boldsymbol{R_p}\,\boldsymbol{R_4}\,\boldsymbol{R_5}\,\boldsymbol{V_{14}^{(0)}} \tag{10.10}$$

3.2.4 Movements of limbs

This subsection describes how the established human body modeling formulates the movements of human limbs. The description starts from the upper limbs, and then followed by the lower limbs. As mentioned in subsection 3.2.3, the main aims of establishing this modeling is to provide a foundation for the development of an improved IK method, as well as to validate the feasibility of building a whole-body model in a universal mathematical software (e.g. MATLAB). Therefore, in this model, the forearm and hand are treated as a single segment, while the lower leg and foot are treated as a single segment.

For the right upper limb, $\alpha_{6,2}$, $\alpha_{6,3}$, $\alpha_{6,4}$, and $\alpha_{7,2}$ (plotted in **Figure 3.3**) are right shoulder flexion/extension, right shoulder abduction/adduction, right shoulder rotation and right elbow flexion/extension. Then, the orientations of right upper arm ($\mathbf{V_6}$) and right forearm ($\mathbf{V_7}$) can be calculated as equation (10.11) and (10.12).

$$\boldsymbol{V_6} = \boldsymbol{R_P}\,\boldsymbol{R_4}\,\boldsymbol{R_6}\,\boldsymbol{V_6^{(0)}} \tag{10.11}$$

$$\boldsymbol{V_7} = \boldsymbol{R_P}\,\boldsymbol{R_4}\,\boldsymbol{R_6}\,\boldsymbol{R_7}\,\boldsymbol{V_7^{(0)}} \tag{10.12}$$

Where $\mathbf{V_6^{(0)}}$ and $\mathbf{V_7^{(0)}}$ are initial orientations of right upper arm and right forearm, in the neutral standing posture, respectively. (For the right elbow ($\mathbf{X_7}$), $\alpha_{7,3} = \alpha_{7,4} = 0$. If we substitute this into equation (9.3), we can get the result that $\mathbf{R_z}(\alpha_{7,3}) = \mathbf{R_z}(\alpha_{7,4}) = \mathbf{I}$ (In this thesis, $\mathbf{I}$ represents the identity matrix). Therefore, by means of substituting this result into equation (9.1), $\mathbf{R_7} = \mathbf{R_y}(\alpha_{7,2})$.)

Similarly, for the left upper limb, we can also have

$$\boldsymbol{V_{12}} = \boldsymbol{R_P}\,\boldsymbol{R_4}\,\boldsymbol{R_{12}}\,\boldsymbol{V_{12}^{(0)}} \tag{10.13}$$

$$\boldsymbol{V_{13}} = \boldsymbol{R_P}\,\boldsymbol{R_4}\,\boldsymbol{R_{12}}\,\boldsymbol{R_{13}}\,\boldsymbol{V_{13}^{(0)}} \tag{10.14}$$

When it comes to lower limbs, since the hip joints and shoulder joints are both socket-ball joints, while the knee joints and elbow joints are both cylinder joints, the kinematic structure of lower limbs is mathematically equivalent to that of upper limbs. Therefore, based on the same mechanism as upper limbs, lower-limb segmental vectors (the left thigh vector ($\mathbf{V_9}$), right thigh vector ($\mathbf{V_2}$), left lower-leg-and-foot vector ($\mathbf{V_{10}}$), as well as the right lower-leg-and-foot vector ($\mathbf{V_1}$)) are calculated as equations (10.15) (10.16) (10.17) and (10.18), respectively.

$$\boldsymbol{V_9} = \boldsymbol{R_P}\,\boldsymbol{R_9}\,\boldsymbol{V_9^{(0)}} \tag{10.15}$$

$$\boldsymbol{V_2} = \boldsymbol{R_P}\,\boldsymbol{R_3}\,\boldsymbol{V_2^{(0)}} \tag{10.16}$$

$$\boldsymbol{V_{10}} = \boldsymbol{R_P}\,\boldsymbol{R_9}\,\boldsymbol{R_{10}}\,\boldsymbol{V_{10}^{(0)}} \tag{10.17}$$

$$\boldsymbol{V_1} = \boldsymbol{R_P}\,\boldsymbol{R_3}\,\boldsymbol{R_2}\,\boldsymbol{V_1^{(0)}} \tag{10.18}$$

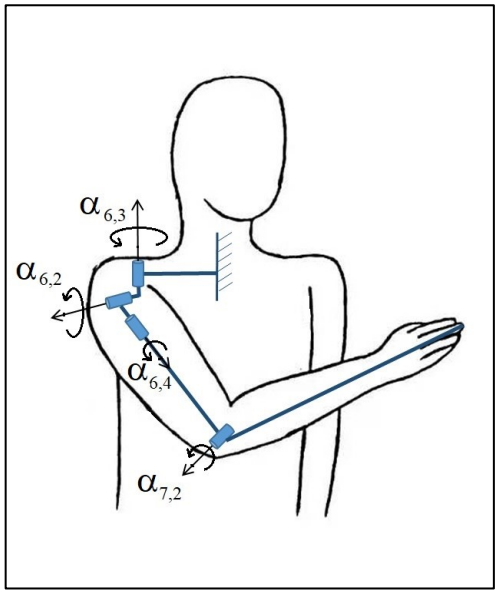

Figure 3.3 Kinematic structure of the right upper limb.

Eventually, if we substitute the equation set 10 (from equation (10.3) to equation (10.18)) into equation set 8, the motion equation set of a simplified entire-body modeling will be completely established.

Chapter 4 Methodology

This chapter introduces how the previous AIK method and the body posture optimization are combined. Furthermore, this chapter also analyzed the performance of present objective functions, and developed a bi-criterion objective function. The combination between AIK method and body posture optimization is an important target of this research, which is expected to combine the solving efficiency of AIK methods with the accuracy of body posture optimization. The other target of this research is to develop an objective function with comprehensive physical meaning, attempting to have a deeper view on the mechanism of the determination of human body posture.

4.1 Analytic inverse kinematic method

Molla and Boulic proposed a singularity-free AIK method, named as Middle Rotation Axis (MRA). Their method can be divided into three steps: i) Determine the elbow flexion; ii) Bring the end-joint (wrist) to the target position; iii) Determine the mid-joint (elbow) position by satisfying the shoulder joint limit and wrist joint limit. [19]

In this research, the MRA-AIK method is achieved by four steps (**Figure 4.1**). The first step solves the elbow flexion angle. As illustrated by Tolani et al, once the target point position is given, then the value of the elbow flexion angle will be purely dependent on the distance between the shoulder joint center and the target point [16]. (Similar with previous research [16] [18] [19], in this thesis, Cosine Law is applied to calculate the elbow flexion angle ($\alpha_{7,2}$), as described in equation (12.1).) Next, the shoulder abduction/adduction angle ($\alpha_{6,3}$) is solved in step 2, according to equation (12.2), where x_6 and y_6 are the x and y coordinates of the shoulder joint position $\mathbf{X_6}$,

respectively; while x_t and y_t are the x and y coordinates of the target point position **T**. After this step, the upper arm, the lower arm, and the target point will be moved into the same plane.

The shoulder flexion angle ($\alpha_{6,2}$) is solved in step 3, according to equation (12.3), where $\mathbf{d_t'}$ and $\mathbf{d_t}$ are vectors pointing from the right shoulder joint centre ($\mathbf{X_6}$) to the 2nd right fingertip ($\mathbf{X_8}$) (determined in step 2) and the target point position **T**, respectively. This step moves the finger tip to the target point.

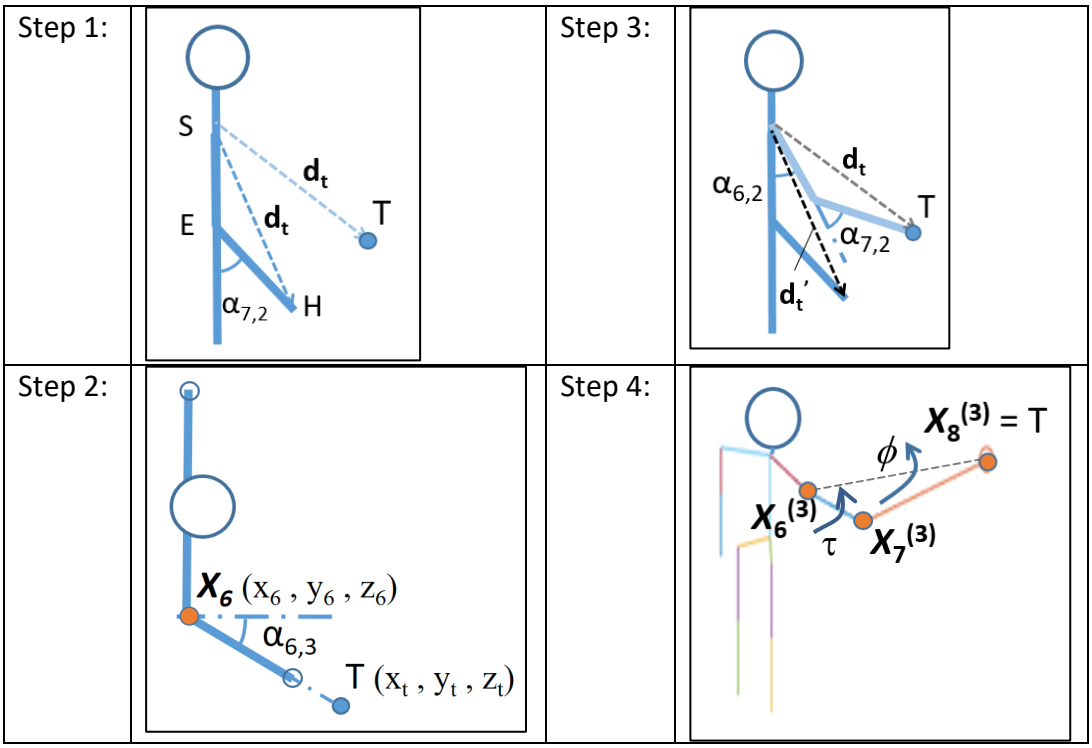

Figure 4. 1 Four steps of the implemented MRA-AIK method in this research. (The notation S, E and H notes the shoulder joint centre, elbow joint centre and the third finger tip of right hand, respectively, while T represents the position of the target point.)

$$\alpha_{7,2} = \cos^{-1}\left(\frac{\boldsymbol{d_t}\cdot\boldsymbol{d_t}-\boldsymbol{V_6}\cdot\boldsymbol{V_6}-\boldsymbol{V_7}\cdot\boldsymbol{V_7}}{2\sqrt{\boldsymbol{V_6}\cdot\boldsymbol{V_6}}\sqrt{\boldsymbol{V_7}\cdot\boldsymbol{V_7}}}\right) \tag{12.1}$$

$$\alpha_{6,3} = \tan^{-1}[(y_t - y_6) / (x_t - x_6)] \tag{12.2}$$

$$|\alpha_{6,2}| = \cos^{-1}[(\boldsymbol{d_t}\cdot\boldsymbol{d_t}') / (\boldsymbol{d_t}\cdot\boldsymbol{d_t})] \tag{12.3}$$
$$(\text{If } x_8 < x_t\ ,\ \alpha_{6,2} = |\alpha_{6,2}|;\ \text{Else},\ \alpha_{6,2} = -|\alpha_{6,2}|.)$$

The swivel angle ϕ is activated in the 4th step (**Figure 4.1**). Based on Euler's Rotation Theorem [28], a function R_{ERT} (**e**, ϕ) is defined in equation (12.6), in order to calculate the rotation matrix of the entire upper limb in the 4th step. In equation (12.6), "**I**" represents the identity matrix. [**e**]* represents an operation, which transfer an arbitrary unit vector e to a matrix [**e**]*, as expressed in equation (12.7). The prime symbol (') represents transfer matrix.

Generate the right elbow position $\boldsymbol{X_7}$:

$$\boldsymbol{\mu} = \boldsymbol{X_8^{(3)}} - \boldsymbol{X_6^{(3)}} \qquad (12.4)$$

$$\boldsymbol{e_\mu} = \boldsymbol{\mu} / \sqrt{\boldsymbol{\mu} \cdot \boldsymbol{\mu}} \qquad (12.5)$$

Euler's Rotation Theorem:

$$R_{ERT}(\boldsymbol{e}, \phi) = \boldsymbol{I} \cos\phi + [\boldsymbol{e}]^* \sin\phi + (\boldsymbol{e}\,\boldsymbol{e}')(1 - \cos\phi) \quad \ldots\ldots (12.6)$$

$$[\boldsymbol{e}]^* = \begin{bmatrix} 0 & -e_z & e_y \\ e_z & 0 & -e_x \\ -e_y & e_x & 0 \end{bmatrix} \qquad \ldots\ldots (12.7)$$

Re-determine shoulder flexion $\alpha_{6,2}$ and shoulder abduction $\alpha_{6,3}$:

$$\alpha_{6,2} = \tan^{-1}\left(\frac{\sqrt{(x_6 - x_7)^2 + (y_6 - y_7)^2}}{z_6 - z_7}\right) \qquad \ldots\ldots (12.8)$$

$$\alpha_{6,3} = \tan^{-1}[(y_4 - y_6) / (x_7 - x_6)] \qquad \ldots\ldots (12.9)$$

When the swivel angle ϕ increases from 0 to ϕ_{lim} degree (ϕ_{lim} represents the upper limit value of the swivel angle ϕ; as shown in the pseudocode in **Figure 4.2**), the shoulder flexion angle ($\alpha_{6,2}$) and shoulder abduction angle ($\alpha_{6,3}$) are calculated by equation (12.8) and (12.9), respectively. Then, the shoulder rotation angle $\alpha_{6,4}$ (marked as τ in the schematic (**Figure 4.1**) and pseudocode (**Figure 4.2)**) increases from 0 to τ_{lim} degree, until the 2nd right fingertip reaches the target position.

The criterion is set as $y_8 > y_t$ (when the 2nd right fingertip crosses the target point, from the right to the left).

Eventually, for each value of the swivel angle ϕ, the value of the objective function f_{obj} will be calculated by substituting the determined set of joint positions ($\mathbf{X}$) and joint angles (α) (as shown in the pseudocode of **Figure 4.2**).

Pseudocode: (Step 4)

For $\phi = 0 \sim \phi_{lim}$

  $\mathbf{R}_\mu = R_{ERT}(\boldsymbol{e}_\mu, \phi)$

  $\boldsymbol{V}_6^{(4)} = \mathbf{R}_\mu \boldsymbol{V}_6^{(3)}$

  Re-calculate $\alpha_{6,3}$, based on equation (12.2)

  Re-calculate $\alpha_{6,2}$, based on equation (12.3)

  Determine the shoulder rotation angle $\alpha_{6,4}$:

  for $\tau = 0 \sim \tau_{lim}$

    if $y_8 > y_t$

      break

    end

  end

  $f_{obj} = f_{obj}(\boldsymbol{X}, \alpha)$

end

Figure 4. 2 Pseudocode of the fourth step of the implemented MRA-AIK method.

4.2 Body Posture Optimization (BPO)

4.2.1 Variable and constraints

An improved upper limb posture determination method is then developed by merging body posture optimization into the third step of MAR-AIK method (noted as "step 4" in **Figure 4.3**, since the second step of the AIK method is divided into two sub-steps). Based on MAR, the optimization variable for reaching tasks is deduced from a set of joint angles (shoulder adduction, shoulder flexion, shoulder rotation and elbow extension) to only one variable, the swivel angle ϕ.

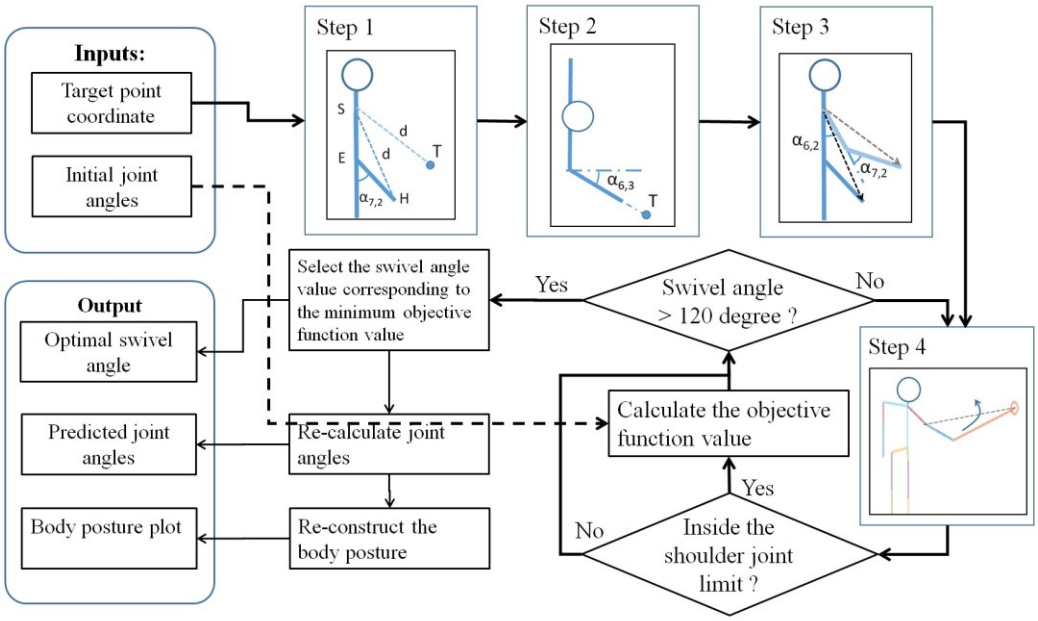

Figure 4. 3 Workflow of the developed AIK method (The notation S, E and H notes the shoulder joint centre, elbow joint centre and the third finger tip of right hand, respectively, while T represents the position of the target point.)

Two constraints are applied in this optimization problem. The first one is the shoulder joint limit. In this research, the shoulder joint limit model proposed by Grassia [29] is applied. Grassia proposed an exponent map (swing and twist angles) as shown in **Figure 4.4**, where the z axis

points the neutral direction of the range of shoulder joint limit [29]. In this research, the neutral direction is determined based on the parameters provided by Engin and Chen [30]. The x axis is inside a vertical plane and perpendicular to the z axis, while the y axis is perpendicular to both the x axis and y axis [29].

To be specific, if we mark the three unit vectors, in the x, y and z directions of the shoulder joint coordinate system, as $\mathbf{e_{sx}}$, $\mathbf{e_{sy}}$ and $\mathbf{e_{sz}}$, respectively; then, $\mathbf{e_{sx}} = (0, 0, 1)^T$, $\mathbf{e_{sy}} = (0, -1, 0)^T$, $\mathbf{e_{sz}} = (1, 0, 0)^T$ (here "^{T}" represent the transferring operation for matrices). Then, if we mark the three unit vectors, in the x, y and z directions of the joint limit coordinate system, as $\mathbf{e_{jx}}$, $\mathbf{e_{jy}}$ and $\mathbf{e_{jz}}$, respectively; then the three axis directions of the joint limit coordinate system ($X_jY_jZ_j$, shown in **Figure 4.4**) can be calculated by equation (13.1), (13.2) and (13.3), where ϕ_n and θ_n are two orientation angles indicating the neutral direction of the shoulder joint (Z_j), defined by Engin and Chen [30], with values of 59 degree and 21 degree, respectively.

$$\boldsymbol{e}_{\mathbf{jx}} = \boldsymbol{R}_{\mathbf{z}}(-\phi_n)\ \boldsymbol{R}_{\mathbf{y}}(\theta_n)\ \boldsymbol{e}_{\mathbf{sx}} \tag{13.1}$$

$$\boldsymbol{e}_{\mathbf{jy}} = \boldsymbol{R}_{\mathbf{z}}(-\phi_n)\ \boldsymbol{R}_{\mathbf{y}}(\theta_n)\ \boldsymbol{e}_{\mathbf{sy}} \tag{13.2}$$

$$\boldsymbol{e}_{\mathbf{jz}} = \boldsymbol{R}_{\mathbf{z}}(-\phi_n)\ \boldsymbol{R}_{\mathbf{y}}(\theta_n)\ \boldsymbol{e}_{\mathbf{sz}} \tag{13.3}$$

The vector **d** is in the direction of the upper arm, with a scale equal to the swing angle value (The swing angle is defined as shown by the hollow arrow in **Figure 4.4**. In this research, the unit of the shoulder swing is degree.) [29]. Then the vector **d** is projected on the x_j –y_j plane (The origin o is the center of shoulder joint.). (To be specific, if we name the projective vector of vector **d**, on the coordinate direction Z_j , as vector $\mathbf{d_z}$, and define the projective vector of vector **d**, on the x_j – y_j plane, as vector $\mathbf{d_{xy}}$, then $\mathbf{d_{xy}}$ can be calculated as $\boldsymbol{d}_{xy} = \boldsymbol{d} - \boldsymbol{d}_z$.) s_x and s_y are the two components of the projection, which are defined as two components of the shoulder swing angle. The shoulder

twist (i.e. shoulder rotation) is then described as a rotation angle around the vector **d**. in this way, the shoulder joint limit is modelled as two parts: swing limit and twist limit. The swing limit proposed by Grassia is shown by equation (14). When the shoulder swing is inside its limit, the value of function f will be negative. [29]

$$f(s_x, s_y) = (s_x / r_x)^2 + (s_y / r_y)^2 - 1 \quad (14)$$

r_x and r_y describe the maximum values of s_x and s_y. Typical values of r_x and r_y are 95 degree and 31 degree, respectively [31]. However, in this research, it is found that, when r_y = 31 degree, the possible range of shoulder rotation will not cover all the experimental values in [1]. Therefore, r_y is increase to 60 degree. The twist limit is modelled as the upper and lower limit of shoulder rotation [29]. According to the publication of Marler et al [2], in this research, the upper and lower limit of shoulder rotation are set as 130 degree and 0 degree, respectively, where internal rotation is positive.

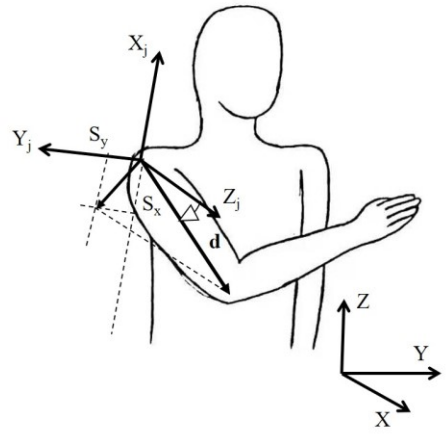

Figure 4. 4 The shoulder swing angle and its x and y components (S_x and S_y, respectively). (X, Y and Z (on the right bottom) indicate the coordinates of the global coordinate system, while X_j , Y_j and Z_j indicate the coordinates of the shoulder joint coordinate system for the shoulder joint limit model) (reference: [31][30])

Another constraint is also added, which is that the swivel angle ϕ cannot go beyond 120 degree. The reason for adding this constraint is that, based on the definition of the swivel angle (as shown in **Figure 2.2**), a swivel angle larger than 120 degree is obviously unnatural. It is worth to point out that the distance constraint [2], which requires the end-effector to reach the target point, is satisfied by the first two steps of the AIK method (from step 1 to step 3 of the **Figure 4.1** and **Figure 4.3**, the second step of the AIK method is divided into two sub-steps in **Figure 4.1** and **Figure 4.3**). Therefore, this constraint is no longer involved in the optimization problem.

4.2.2 Combination between MRA-AIK and BPO

As shown in **Figure 4.3,** the optimization module is merged to the fourth step of the MRA-AIK method. In the fourth step, the swivel angle is increased from 0 to 120 degree, with a step of 1 degree. For each swivel angle value, it will be initially examined if the upper arm is inside the shoulder joint limit (This thesis applied the shoulder joint limit model proposed by Grassia)[29]. The inputs of this developed method are the target point position and initial upper limb posture. (The initial upper limb posture data will be utilized when the objective function is the joint displacement function.) Then, if the upper arm is inside the shoulder limit, the objective function value will be calculated.

Finally, the swivel angle value, corresponding to the minimum objective function value, will be initially output. Then, the joint angles will be re-calculated, based on the value of the swivel angle. Based on re-calculated upper limb joint angle values, the positions of upper limb joint centers will be calculated, and the predicted upper limb posture will be re-constructed and plotted out.

4.3 Simulation of previous objective functions

The feasibility of the joint displacement function and joint discomfort function is primarily judged by the experiment results of Admiraal et al [1], whose extracted data has also been utilized by Kashi et al [23]. Nine subjects are involved in the experiment of Admiraal et al. while five target points are set up, thus twenty couples of initial and final target points are studied.

Admiraal et al quantified human arm postures by the rotational angle of shoulder. In this simulation, measured shoulder rotation values are plotted, versus those shoulder rotation values, predicted by applying the joint discomfort function and joint displacement function, respectively. In each plot, a straight blue line, with a slope equal to one, is plotted, which indicates "measured value = predicted value".

joint weights of joint displacement function are cited from the publication of Zou et al [26], while the joint discomfort function is cited from the publication of Marler et al [21]. The delta potential energy function is not involved since it will always lead to the smallest swivel angle value.

4.4 Proposed bi-criterion objective function

Further simulation was conducted on the joint discomfort function, joint displacement function and delta potential energy function, for the five target points selected in the experiment of Admiraal et al [1]. Since joint discomfort curves are "well-shaped"(changes rapidly on the "wall" of these "well", but slightly on the "bottom" of these "well") (shown in **section 4**), a bi-criterion objective function ($f_{discomf\text{-}displace}$) has been proposed by adding joint discomfort and joint

displacement together (shown in equation (15)), where α is the coefficient of the discomfort function.

$$f_{discomf\text{-}displace} = \alpha \bullet f_{discomf} + f_{displace} \quad (15)$$

Then, on the "wall" of these "well", the value of this new objective function will be dependent on joint discomfort, while, on the bottom of these "well", the value of this new objective function will be mainly determined by joint displacement. Therefore, by means of this, the predicted shoulder rotation value, for each couple of initial target point and final target point, will be limited into a relatively small range, and become more accurate.

4.5 Linear regression and suboptimal coefficient value

For an ideal inverse kinematic method, for each couple of initial target point and final target point, the determined shoulder rotation value ($\zeta_{predicted}$) should be equal to the measured shoulder rotation value ($\zeta_{measured}$) (i.e. $\zeta_{predicted} = \zeta_{measured}$), which is a linear relation. Therefore, linear regression is applied to estimate the accuracy of the shoulder rotation values, determined by the developed AIK method. Shoulder rotation value residuals ($\zeta_{residual}$) are calculated as the difference between the measured values ($\zeta_{measured}$) and linear regression values ($\zeta_{regression}$) (shown in equation (16)). A residual analysis is then conducted by plotting the average residual values, among the 9 subjects, involved in the experiment of Admiraal et al [1], in order to compare the performance of the bi-criterion objective function and joint discomfort function, based on the developed AIK method. Coefficient of determination (R^2) (shown in equation (17) [32]) is also calculated to quantify the accuracy of the shoulder rotation values, determined by the developed AIK method.

$$\zeta_{residual} = \zeta_{measured} - \zeta_{regression} \tag{16}$$

Where, $\zeta_{measured}$ is the measured value (unit: degree).

$\zeta_{regression}$ is the linear regression value (unit: degree).

$$R^2 = 1 - SSR/TSS \tag{17}$$

Where, SSR is the Sum of Squares of Residuals ($\zeta_{residual}$);

TSS is the Total Sum of the Squares of linear regression values ($\zeta_{regression}$).

In equation (15), if α keeps increasing, then $f_{discomf\text{-}displace}$ will eventually become equivalent to $f_{discomf}$. On the contrary, if α becomes zero, then $f_{discomf\text{-}displace}$ will become $f_{displace}$. Based on the research of Admiraal et al, body postures are determined by the final target point position and the initial body posture together [1]. However, the minimization of the joint discomfort function does not reflect the effect of the initial body posture. Therefore, theoretically, when α keeps increasing, the accuracy of predicted shoulder rotation values will not keep increasing but start decreasing at a certain point. In this way, for a certain database, the coefficient of determination (R^2) will become a function of the coefficient of the discomfort function (α) (as shown in equation (18)), and the domain of α is from zero to positive infinite. Furthermore, theoretically, a suboptimal value of α (α_{opt}) exists between zero and infinite.

$$R^2 = R^2(\alpha) \tag{18}$$

A pilot search is initially conducted. The starting value of α is set to be 10^{-14}, by the best guess. Then the coefficient value is magnified/divided by 100, and α values of 10^{-16} and 10^{-12} are

attempted. A step of 4 is set for the power number of α. Then a golden section search [33] is applied in the interval (0.0001, 10000), to find out the suboptimal coefficient value (α_{opt}).

4.6 Case study

A case study is conducted to show the application of this improved IK method in ergonomic risk assessment. The body postures of the key frames of the assumed case are determined by the improved IK method. Then, based on the determined body postures (i.e. joint angles), corresponding ergonomic risk is calculated as the RULA risk score [37].

The case is assumed that a worker is appointed to do assembling work on a table. After this work, he would clear the table and put his tools back to his toolbox. It is assumed that, during the assembling work, he would use two tools, tool A and tool B. The positions of tool A and tool B, when he finishes the assembling work, are as shown in **Figure 4.5 (c)**. Two selective positions (point E and F shown in **figure 4.5**) are designed to put his toolbox. This case study focuses on the procedure of putting back the tools. In order to clear his working table, he would move tool A first back to the toolbox, then return tool B to the toolbox. The target in this case study is to select an ergonomically friendly position for him to place the toolbox. It is also assumed that his height is 1.8 meters, while this worker is right-handed.

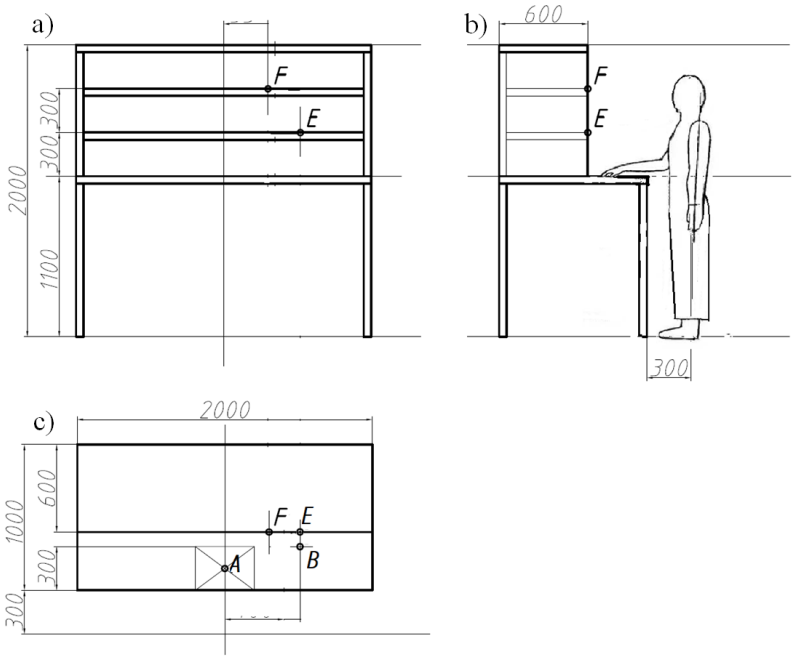

Figure 4. 5 Sketch of the assumed case: a) back view; b) side view; c) top view.

According to the case description, this simulation starts from the end of the assembling task, when the right hand is inside the working area, and the tool A is in the right hand. Thus, the starting posture is set as reaching the center of the working area, in order to represent the whole working area. Therefore, this case can be modelled as the following motion sequence: This table-cleaning task starts from step 1 - reaching the central point of the working area (point A), and then step 2 - reaching the toolbox (target point E or F), and then step 3 - reaching the second tool (point B), and finally step 4 - reaching the toolbox (target point E or F) again (put the second tool back to the toolbox).

Chapter 5 Results and discussion

This section shows the comparison between the shoulder rotation values, predicted by the joint discomfort function, joint displacement function and proposed bi-criterion objective function, respectively, and the shoulder rotation values measured by Admiraal et al [1]. The simulation result of the joint discomfort function, joint displacement function and delta potential energy function is also shown in this section.

5.1 Simulation on previous cost functions

Figure 5.1 shows the value of joint discomfort, joint displacement and delta potential energy, changing with the swivel angle, within joint limit, which provides further accordance for the combination of the joint discomfort function and joint displacement function (as discussed in section 3.3). The five target points are cited from the publication of Admiraal et al [1]. For the joint displacement function and delta potential energy function, the initial posture in this simulation is neutral standing.

As shown in **Figure 5.1**, joint discomfort curves are "well-shaped". Therefore, by adding the joint discomfort function to the joint displacement function, the predicted shoulder rotation value is expected to be limited in a more accurate range.

5.2 Proposed bi-criterion objective function

Figure 5.2 plots the measured shoulder rotation values [1], versus the shoulder rotation values, determined by applying proposed objective function with different coefficient values. **Figure 5.2 (a)** shows the performance of the joint displacement function (The proposed bi-

criterion objective function is equal to the joint displacement function when the coefficient value is zero.). As shown in **Figure 5.2 (a),** the majority of the data points spread in a triangular area, which shows that there is no obvious relation between the predicted shoulder rotation values and measured values. This result is different from the result of Zou et al. In the research of Zou et al, the joint displacement function predicts reasonable body postures [26]. This phenomenon indicates that an IK method, validated by whole-body reaching motion, is possible to be inaccurate when the torso is fixed.

It is shown that, as the value of the coefficient of the joint discomfort function increases, data points gradually gathered into several columns. This phenomenon is caused by the fact that the joint discomfort function does not consider the effect of the initial posture, while the joint displacement function considers it. When the effect of the initial posture is neglected, the measured shoulder rotation values, with different starting target points, will be matched with the same predicted value. Therefore, when the coefficient of the joint discomfort function increases, data points with the same final target point will become closer and closer.

It is also exhibited that, generally, data points get more and more close to the straight blue line, whose slope is one. This blue line indicates the position where the measured value is equal to the predicted value. Therefore, this phenomenon shows that, by adding the joint discomfort function to the joint displacement function, the accuracy is increased indeed.

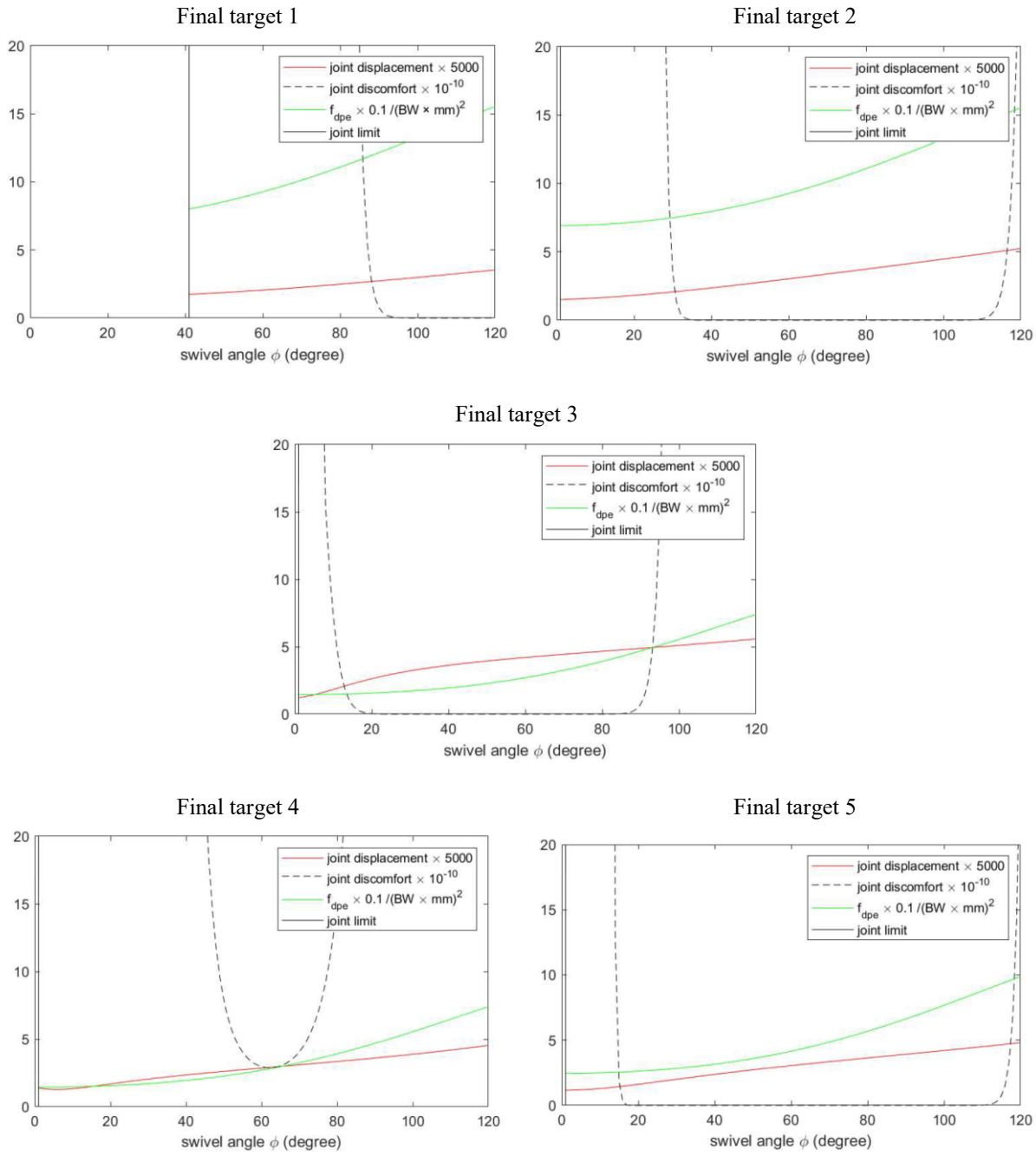

Figure 5. 1 Changes of values of joint displacement, joint discomfort and delta potential energy versus swivel angle, within the shoulder joint limit, at the five selected target points, studied by Admiraal et al [1].

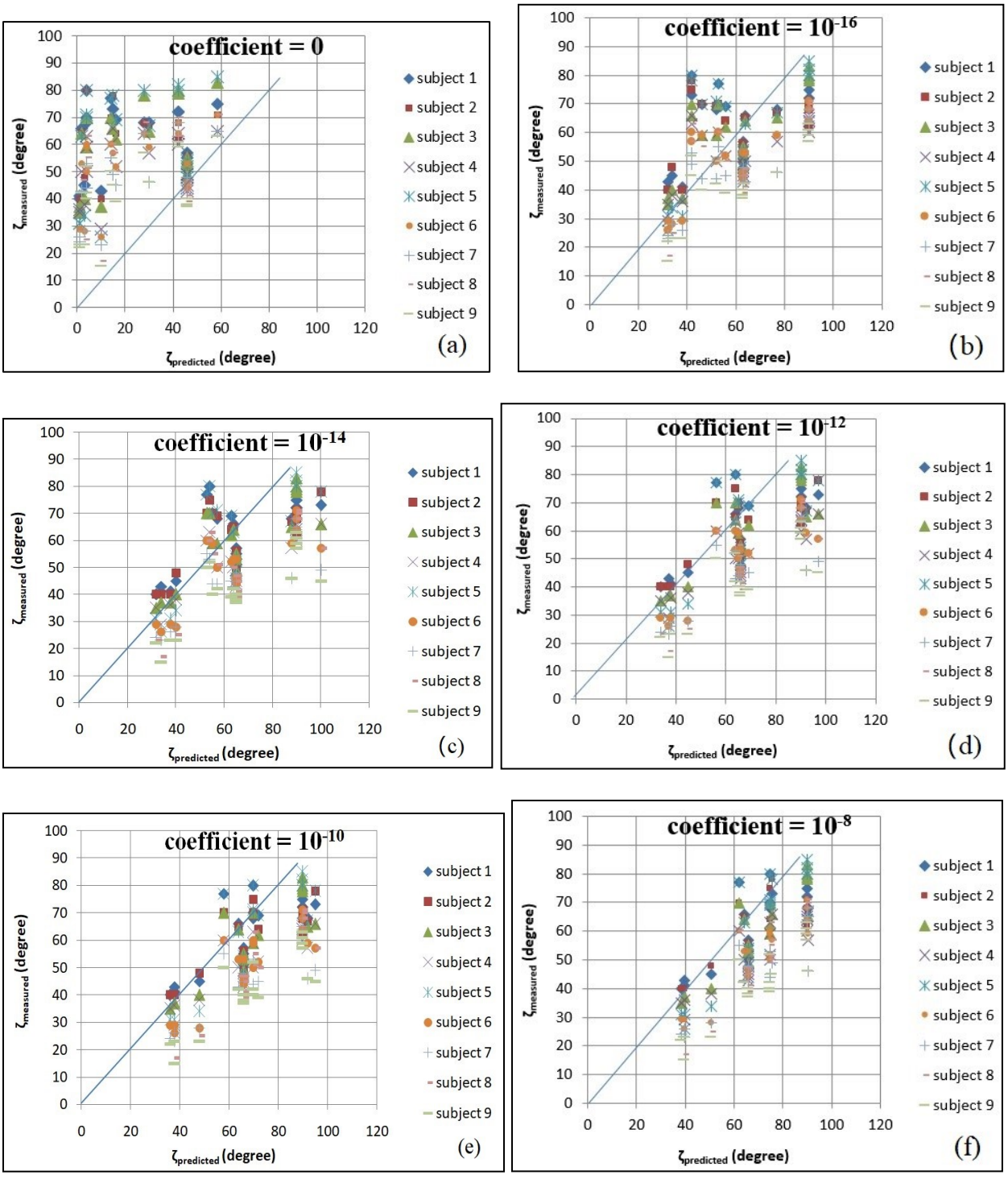

Figure 5. 2 Extracted shoulder rotation values [1] versus the shoulder rotation values, determined by proposed bi-criterion objective function, for different coefficient values.

5.3 Suboptimal coefficient value

Figure 5.3 shows the accuracy of the predicted shoulder rotation values (evaluated by the coefficient of determination), changing by the value of α. As discussed in section 3.6, the search of the optimal value of α consists of two phases -- pilot search and golden section search. **Figure 5.3 (a)** shows the result of the pilot search. As shown in **Figure 5.3 (a),** when the value of α increased from 10^{-16} to 10^{4}, the R^2 value increases first, and then starts decreasing, which agrees with our hypothesis in section 3, and also limits the optimal value of α into the range between 0.0001 and 10000. **Figure 5.3 (b)** shows the result of the golden section search. Based on the golden section search, the optimal α value for the subject 1, 6, 7, 8 and 9 is 13; the optimal α value for the subject 2 is 3; while the optimal value of α, for the subject 3, 4 and 5, is 1. Therefore, the global optimal value of α is determined as the weighted average, which is 7.7.

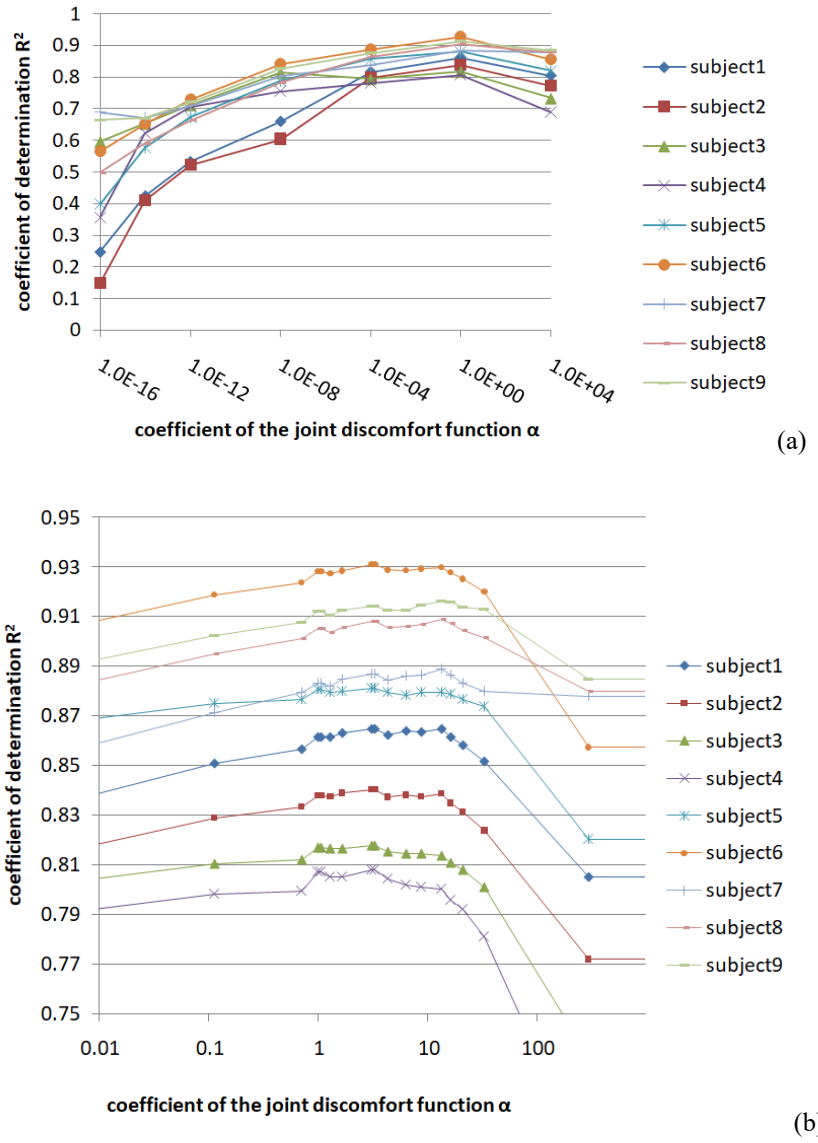

Figure 5. 3 The coefficient of determination values of all the nine subjects, involved in the research of Admiraal et al [1], changing with the value of α. (a) Result of the pilot search; (b) result of the golden section search.

5.4 Performance of the finalized function

This subsection exhibits the performance of the developed AIK method, as well as compares its performance with that of the previous AIK methods. **Figure 5.4** plots the measured shoulder rotation values ($\zeta_{measured}$), versus the values ($\zeta_{predicted}$), determined by different AIK methods.

Subplots (a) and (b) show the results of previous AIK methods. “Previous AIK method 1” refers to the AIK method selecting the smallest swivel angle value, within the shoulder joint limit; while the “previous AIK method 2” refers to the AIK method selecting the middle swivel angle value, within the shoulder joint limit. (This notification of previous AIK methods also works in **Table 2** and **Figure 5.5**) Subplots (c) and (d) shows the results of the developed AIK method, with the joint discomfort function and proposed bi-criterion function (when the coefficient (α) equals to 7.7), respectively.

Table 2 compares the coefficient of determination (R^2) values of the determined shoulder rotation values, determined by previous AIK methods and the developed AIK method, with the joint discomfort function and the proposed bi-criterion objective function. However, the coefficient of determination (R^2) value cannot fully represent the relation that the determine shoulder rotation value ($\zeta_{predicted}$) should be equal to the measured shoulder rotation value ($\zeta_{measured}$) ($\zeta_{predicted} = \zeta_{measured}$) (e.g. the slope of the regression line is not considered.). Therefore, a residual analysis is conducted as an addition. **Figure 5.5** shows the result of the residual analysis, which plots the absolute residual values ($|\zeta_{residual}|$). The red color indicates that the corresponding residual value is positive, while the blue color indicates that is negative.

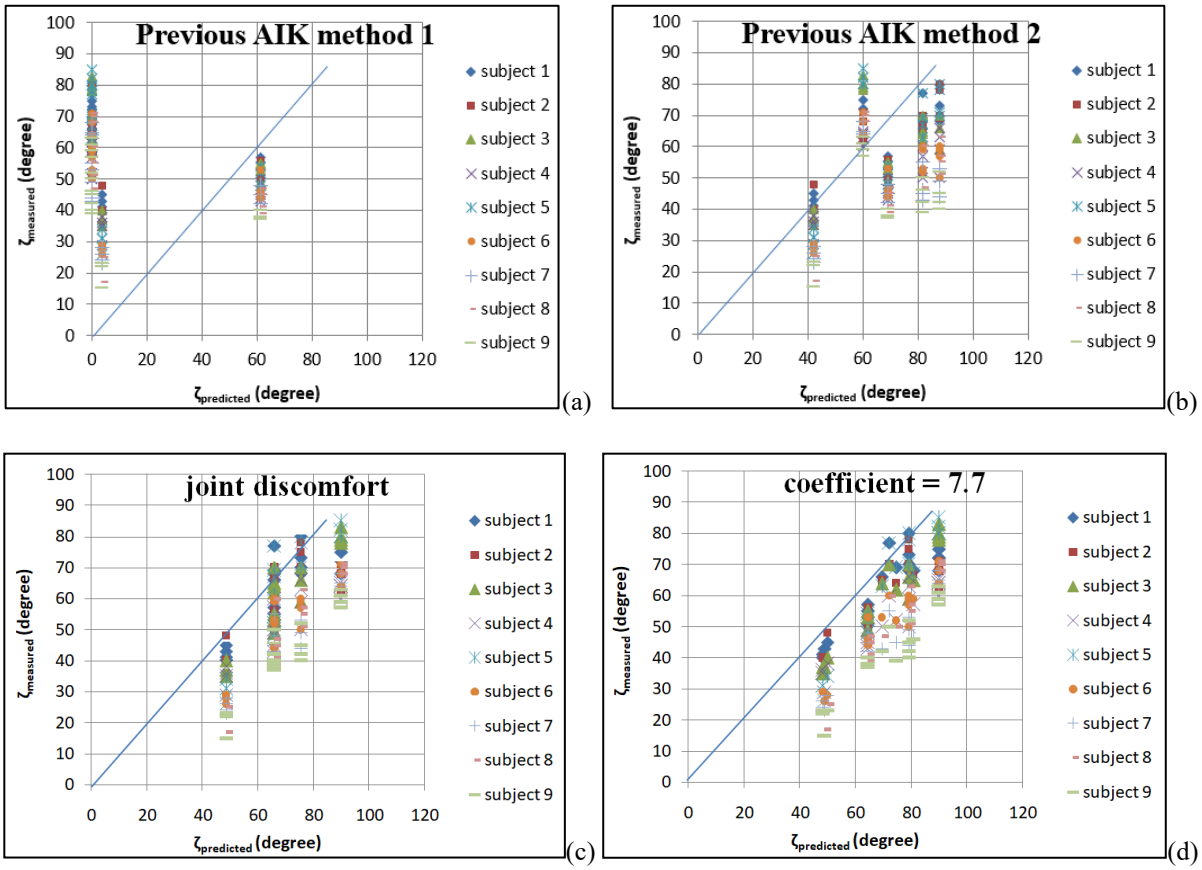

Figure 5. 4 Measured shoulder rotation values ($\zeta_{measured}$), versus the determined values ($\zeta_{predicted}$). (a)"Previous AIK method 1" (selecting the smallest swivel angle value within the shoulder joint limit); (b)"Previous AIK method 2" (selecting the middle swivel angle value within the shoulder joint limit); (c) the developed AIK method with the joint discomfort function; (d) the developed AIK method with the proposed bi-criterion objective function and the suboptimal coefficient value (when the coefficient (α) equals to 7.7).

5.4.1 Comparison between previous AIK methods

As shown in **Figure 5.4**, the data points in **Figure 5.4 (a)** gather in three columns, which does not show a correlation between the measured shoulder rotation values and the shoulder rotation values determined by selecting the lowest swivel angle value, within the shoulder joint limit. On the contrary, the shoulder rotation values determined by the second previous AIK method (selecting the middle value of the swivel angle, within the shoulder joint limit) shows a rough correlation with the measured shoulder rotation values. (As shown in **Figure 5.4 (b)**, the data

points determined by "previous AIK method 2" gather in five columns, which roughly spread around the straight line with a slope of one.)

This difference between the performances of previous AIK methods is also quantified by the coefficient of determination (R^2) value. As shown in **Table 2**, the R^2 value of the result of the "previous AIK method 2" (0.3528) is 228.7 percentage higher than that of the "previous AIK method 1" (0.0823). When it comes to the residual analysis, as shown in **Figure 5.5**, the maximum residual of the "previous AIK method 2" (around 24 degree, shown in **Figure 5.5 (b)**) is lower than that of the "previous AIK method 1" (around 27 degree, shown in **Figure 5.5 (a)**), which also exhibits that accuracy of the "previous AIK method 2" is higher than the "previous AIK method 1". Therefore, based on the comparison above, the "previous AIK method 2" (selecting the middle value of the swivel angle within the shoulder joint limit) is set as a standard to evaluate the performance of the developed AIK method (i.e. the developed AIK method is compared with the "previous AIK method 2" in subsection 4.4.2.).

5.4.2 Comparison between the developed AIK method and previous AIK methods

Figure 5.4 (a) and **(b)** exhibit the determined results of the developed AIK method, with the joint discomfort function and the proposed bi-criterion function, respectively. Compared with the "previous AIK method 2" (**Figure 5.4 (b)**), almost all the data points, determined by the developed AIK method, with both the joint discomfort function (**Figure 5.4 (c)**) and the proposed bi-criterion function (**Figure 5.4 (d)**) locate under the straight line with a slope of one. Moreover, the top of each column of data points, in **Figure 5.5 (c)** and **Figure 5.5 (d)**, is either on or close to the straight line with a slope of one, which shows that the tendency of the determined result of the developed AIK method is very close to the relation that "$\zeta_{predicted} = \zeta_{measured}$".

Table 2 Coefficient of determination (R^2) values of the determined shoulder rotation angle values, by the previous AIK methods and the developed AIK method (with the proposed bi-criterion objective function (with optimal coefficient value (α_{opt})) and the joint discomfort function ($f_{discomf}$), respectively).

Subject	R^2 (Previous AIK method I)*	R^2 (Previous AIK method II)**	R^2 ($f_{discomf}$)	R^2 (α_{opt})
1	0.1663	0.3492	0.8050	0.8636
2	0.1770	0.3523	0.7719	0.8375
3	0.1252	0.5283	0.7326	0.8144
4	0.0783	0.4860	0.6888	0.8011
5	0.0588	0.3496	0.8200	0.8793
6	0.0568	0.3294	0.8573	0.9292
7	0.0400	0.3403	0.8777	0.8866
8	0.0118	0.2271	0.8798	0.9070
9	0.0264	0.2127	0.8847	0.9146
Mean value	0.0823	0.3528	0.8131	0.8704

*Selecting the smallest swivel angle value within the shoulder joint limit;

**Selecting the middle value of the swivel angle, within the shoulder joint limit.

This increase of the accuracy is also shown by the coefficient of determination (R^2) (**Table 2**). As shown in **Table 2**, with the joint discomfort function, the developed AIK method determined shoulder rotation values with an R^2 value of 0.8131, which is 130.5 percent higher that of the "previous AIK method 2" (0.3528). Moreover, the developed AIK method, with the proposed bi-criterion function (with the suboptimal coefficient value), determined shoulder rotation values with an R^2 value of 0.8704, which is 146.7 percent higher than the "previous AIK method 2". When it

comes to the residual analysis, the maximum residual of the developed AIK method, with the joint discomfort function, is around 15 degree (shown in **Figure 5.5 (c)**); while the maximum residual with the proposed bi-criterion function is around 10 degree (shown in **Figure 5.5 (a)**). Compared with the "previous AIK method 2" (whose maximum residual is about 24 degree), the maximum residual values of the developed AIK method, with the joint discomfort function and the proposed bi-criterion function, decrease by approximately 37.5% and 58.3%, respectively. This result shows that, by means of combining the previous AIK method with a body posture optimization module, the accuracy of the MRA-AIK method, in the determination of upper limb postures, is obviously improved.

5.4.3 Comparison within the developed AIK method

As shown in **Table 2**, for all the nine subjects, the proposed objective function with the suboptimal coefficient value (which is 7.7) determines more accurate shoulder rotation values. To be specific, the average coefficient of determination (R^2) value, corresponding to the proposed objective function is 0.8704, increasing by 0.0573 (7%) from the R^2 value corresponding to the joint discomfort function. It is also shown that, compared with the joint discomfort function, the proposed bi-criterion objective function decreases the inaccuracy of the prediction at final target 5. These two phenomena show that, by means of combining the joint discomfort function and the joint displacement function, as well as searching the suboptimal coefficient value for the proposed bi-criterion objective function, the performance of the developed AIK method is further improved.

It is also shown that, for the proposed bi-criterion objective function with the suboptimal coefficient value, data points spread into seven columns; while the data points determined with the joint discomfort function gather in 4 columns. This comparison also shows the advantage of the

proposed bi-criterion objective function and the searched suboptimal coefficient value. However, since the proposed objective function involves the joint displacement function, it considers the effect of initial postures and should theoretically have 20 columns in the "measured value - predicted value" plot. Thus the proposed objective function still has potential to be improved.

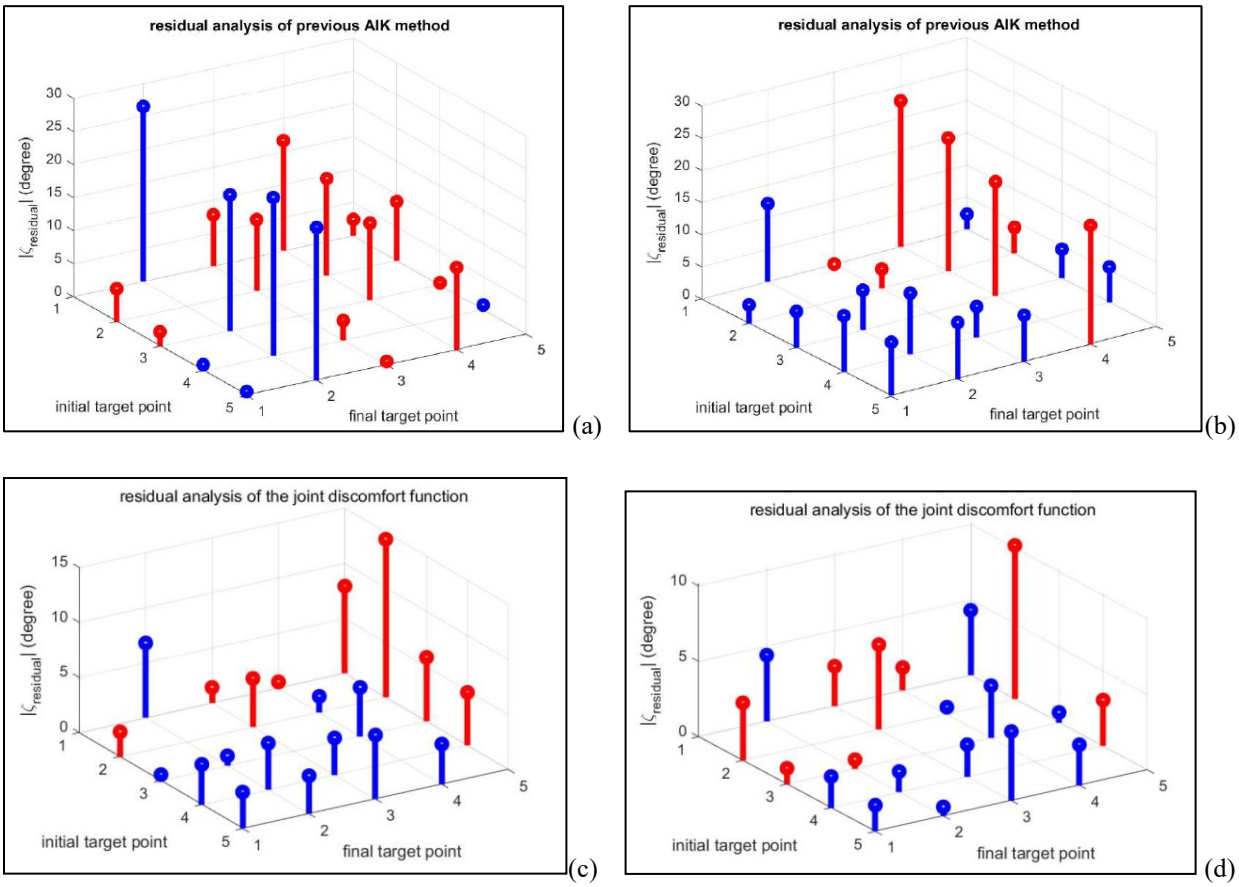

Figure 5. 5 Residual analysis for the previous AIK methods and the developed AIK method. (a)"Previous AIK method 1" (selecting the smallest swivel angle value within the shoulder joint limit); (b)"Previous AIK method 2" (selecting the middle swivel angle value within the shoulder joint limit); (c) the developed AIK method with the joint discomfort function; (d) the developed AIK method with the proposed bi-criterion objective function and the suboptimal coefficient value (when the coefficient (α) equals to 7.7).

5.5 Case study

When it comes to the case study (described in **subsection 4.6**), **Figure 5.6** exhibits the determined body postures. As shown in **Figure 5.6**, the body posture in the second step, of both scenarios I and II, are different from those of the fourth step, which exhibits the effect of the joint

displacement component, in the proposed bi-criterion objective function, on the result of body-posture determination. In addition, as shown in **Figure 5.6**, the body postures of the first step (The first step is reaching the center of the working area), for both scenario I and scenario II, turn out to be the same, which agrees with the expectation (As discussed in the **subsection 4.6** "simulation setup", the starting postures for the scenario I and II should be the same.)

Figure 5.7 shows the ergonomic risk assessment results of this case study. The sum of the total RULA risk scores for scenario I (target point E) and scenario II (target point F) are 19 and 24, respectively. Therefore, between these two target points, target point E is more ergonomically friendly to put the toolbox. Although the target E is on the right side of target F, target E is still more ergonomically friendly than target F, which shows that, in this case, the height of the target point has bigger effect on the ergonomic risk, than the abduction of the target point. In addition, as shown in **Figure 5.7**, the difference of the determined body postures of the step 2 and 4 (shown in **Figure 5.6**), for scenario I, lead to different ergonomic risk scores, which shows the importance of involving the joint displacement function in the objective function.

Although the step 3 of scenarios I and II have different initial postures, the predicted body postures for step 3, in both scenarios I and II, turn out to be the same. The probable reason is that the position of tool B is close to the boundary of the reaching zone, where the "well" of the joint discomfort function is very narrow and the effect of the initial posture (considered in the joint displacement function) is not significant.

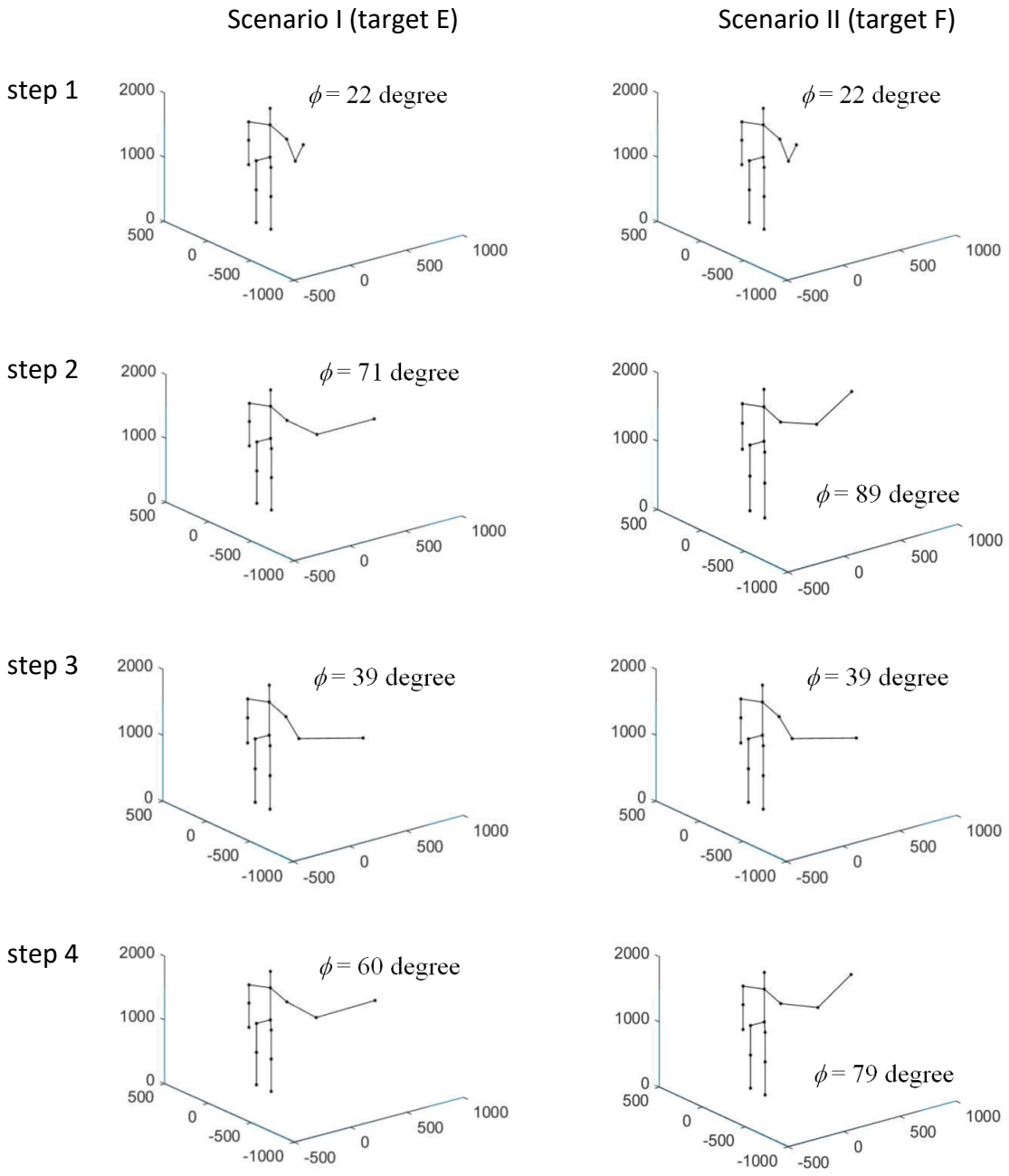

Figure 5. 6 Determined body postures for the two scenarios of the case study. (ϕ is the value of the swivel angle)

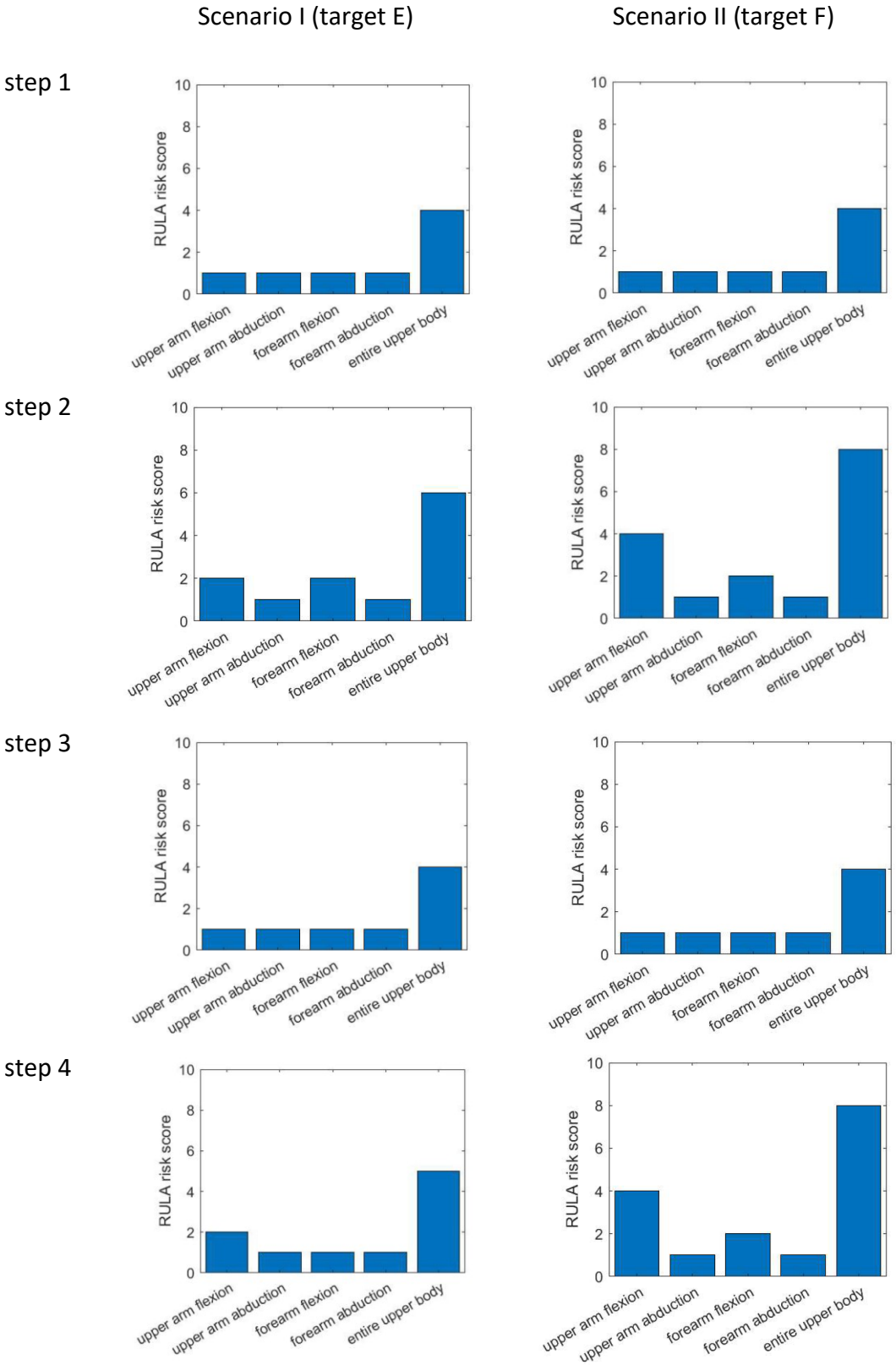

Figure 5. 7 Ergonomic risk assessment result of the two scenarios in the case study.

Chapter 6 Summary and conclusions

This dissertation shows the development of an improved AIK method, which has a wide spectrum of applications, especially in the ergonomic risk assessment. This improvement is based on the MRA-AIK method, and implemented by combining the MRA-AIK method with body-posture optimization. To summarize, this research has five major contributions as listed below.

1. This research combines the MRA-AIK method with body posture optimization, which increased the accuracy of the MRA-AIK method, in the determination of the human upper limb postures during tasks. By means of this combination, the shoulder joint limit model works as a constraint of the body posture optimization problem, which simplified the optimization procedure. Therefore, this combination is also expected to increase the computational efficiency, compared with previous body posture optimization methods.

2. Based on the developed AIK method, an innovative objective function is proposed by combining the joint discomfort function and the joint displacement function. This thesis initially examined the performance of the joint displacement function. Although the joint displacement function predicts reasonable body postures for whole-body reaching tasks, result shows that it does not predict accurate body postures when the torso is fixed.

Based on the developed AIK method, the joint discomfort function predicts reasonable upper limb postures for reaching tasks. However, since it does not reflect the effects of the initial body postures, a bi-criterion objective function is proposed by adding the joint discomfort function and joint displacement function. Compared with previous bi-criterion and multiple objective functions, it is clear to see how the different components work together, in the proposed bi-criterion objective function, which makes our bi-criterion objective function mathematically comprehensive.

Results show that the accuracy of the proposed objective function is satisfactory and higher than both the joint discomfort function and joint displacement function, which not only convinces the performance of the developed AIK method (in the reaching tasks with the fingertip being the end-effector), but also adds to the reliability of the assumption that the natural human body posture is determined by minimizing both the discomfort and energy cost.

3. A systematic approach is applied to determine the coefficient value. This approach is also applicable for any other objective function with two components. In this approach, the coefficient of determination (R^2) is selected to quantify the accuracy of the result of optimization. The determination of the suboptimal value of the coefficient (α) is based on previous published data. The larger data scale we have, the more accurate value of α will we determine. Golden section search is applied to determine the suboptimal value of the coefficient. The program can also be further improved, in order to automatically search for the optimal coefficient value.

4. In order to implement this developed AIK method, a simplified human body model is established in MATLAB, which provides users with higher flexibility. In this model, an adjusted data structure is applied for joint angles, which is more systematic and comprehensive than previous data structure. Although the developed AIK method is established on this human body model, the model itself is independent from the developed AIK method. Therefore, although the developed AIK method is so far only able to determine joint angles of the upper limb, a human body model is still established with all the body segments. Future research can continue to improve the developed AIK method and make it able to determine all the joint angles.

5. The case study exhibits the application of the developed AIK method in proactive ergonomic risk assessment, which does not require the human mimic, and will increase the efficiency of ergonomic risk assessment. This case study shows that, based on the developed

AIK method, the ergonomic risk, on a set of given target points, can be proactively estimated, and compared, which provides important information for ergonomic workplace design. Future improvement can involve the automatic search of all the reachable points, and find out the most ergonomically friendly target point.

Limitations of the developed AIK method are described as follows.

Initially, although the combination between the MRA-AIK method and BPO is supposed to achieve higher computational efficiency, this hypothesis needs to be validated by further research. Secondly, for the determination of the suboptimal coefficient value (α_{opt}), R^2 cannot represent the relation that the determined values should be equal to the measured values. Therefore, other quantities should be applied to replace R^2 in future research, such as the residual. Another limitation of the currently developed AIK method is that the movement of the wrist joint is omitted in the current stage of the developed AIK method. Therefore, the currently developed AIK method is not applicable in those cases when the hand orientation is constrained or limited (for example, when the hand orientation is affected by the geometry of the target or any barrier(s) in the working environment).

In addition, this research only focuses on the reaching task conducted by fingertips, when the torso fixed. Therefore, the suboptimal value of α, determined in this research, will probably change for other tasks. More research is supposed to be conducted on different tasks in the future. Moreover, since the upper limb strength depends on the upper limb posture, the weight of the load in hand can also impact the upper limb posture. In this thesis, only the upper limb posture without a load in hand is discussed. The determination of the upper limb posture with load should be

investigated in future research, while the suboptimal value of the coefficient is supposed to be impacted by the weight of the load.

References

[1] Admiraal MA, Kusters MJMAM, Gielen SCAM. Modeling kinematics and dynamics of human arm movements. Motor Control 2004;8:312–38.

[2] Marler RT, Arora JS, Yang J, Kim HJ, Abdel-Malek K. Use of multi-objective optimization for digital human posture prediction. Eng Optim 2009;41:925–43.

[3] Yang J, Marler T, Rahmatalla S. Multi-objective optimization-based method for kinematic posture prediction: Development and validation. Robotica 2011;29:245–53.

[4] Jung ES, Kee D, Chung MK. Upper body reach posture prediction for ergonomic evaluation models. Int J Ind Ergon 1995;16:95–107.

[5] Wang J, Han SH, Li X. 3D fuzzy ergonomic analysis for rapid workplace design and modification in construction. Autom Constr 2021;123:103521.

[6] Li X, Han S, Gül M, Al-Hussein M, El-Rich M. 3D Visualization-Based Ergonomic Risk Assessment and Work Modification Framework and Its Validation for a Lifting Task. J Constr Eng Manag 2018;144:1–13.

[7] Li X, Han SH, Gül M, Al-Hussein M. Automated post-3D visualization ergonomic analysis system for rapid workplace design in modular construction. Autom Constr 2019;98:160–74. https://doi.org/10.1016/j.autcon.2018.11.012.

[8] Marler T, Knake L, Johnson R. Optimization-based posture prediction for analysis of box lifting tasks. Lect Notes Comput Sci (Including Subser Lect Notes Artif Intell Lect Notes Bioinformatics) 2011;6777 LNCS:151–60. https://doi.org/10.1007/978-3-642-21799-9_17.

[9] Azizi S, Dadarkhah A, Asgharpour Masouleh A. Multi-Objective Optimization Method for Posture Prediction of Symmetric Static Lifting Using a Three-Dimensional Human Model.

Ann Mil Heal Sci Res 2020;In Press. https://doi.org/10.5812/amh.104283.

[10] Parger M, Schmalstieg D, Mueller JH, Steinberger M. Human upper-body inverse kinematics for increased embodiment in consumer-grade virtual reality. Proc ACM Symp Virtual Real Softw Technol VRST 2018. https://doi.org/10.1145/3281505.3281529.

[11] Aristidou A, Lasenby J, Chrysanthou Y, Shamir A. Inverse Kinematics Techniques in Computer Graphics: A Survey. Comput Graph Forum 2018;37:35–58.

[12] Pieper DL. The kinematics of manipulators under computer control. 1969.

[13] Ralph .S M. Handyman-to-Hardiman 1967:12.

[14] Denavit J, Hartenberg RS. A kinematic notation for lower pair mechanisms based on matrices. J Appl Mech 1955;77:215–21.

[15] J. J. Uicker J. Dynamic Force Analysis of Spatial Linkages 1967:418–24.

[16] Tolani D, Goswami A, Badler NI. Real-time inverse kinematics techniques for anthropomorphic limbs. Graph Models 2000;62:353–88.

[17] Fang C, Ajoudani A, Bicchi A, Tsagarakis NG. A Real-Time Identification and Tracking Method for the Musculoskeletal Model of Human Arm. Proc - 2018 IEEE Int Conf Syst Man, Cybern SMC 2018 2018:3472–9. https://doi.org/10.1109/SMC.2018.00588.

[18] Kallmann M. Analytical inverse kinematics with body posture control. Comput Animat Virtual Worlds 2008:271–81. https://doi.org/10.1002/cav.

[19] Molla E, Boulic R. Singularity free parametrization of human limbs. Proc - Motion Games 2013, MIG 2013 2013:165–74. https://doi.org/10.1145/2522628.2522649.

[20] Mi Z, Yang J, Abdel-Malek K. Optimization-based posture prediction for human upper body. Robotica 2009;27:607–20. https://doi.org/10.1017/S0263574708004992.

[21] Marler RT, Rahmatalla S, Shanahan M, Abdel-Malek K. A new discomfort function for optimization-based posture prediction. SAE Tech Pap 2005. https://doi.org/10.4271/2005-01-2680.

[22] Rout B, Tripathy PP, Dash RR, Dhupal D. Optimization of Posture Prediction Using MOO in Brick Stacking Operation. Adv. Intell. Syst. Comput., vol. 990, Springer; 2020, p. 461–72. https://doi.org/10.1007/978-981-13-8676-3_40.

[23] Kashi B, Avrahami I, Rosen J, Brand M. A Bi-Criterion Model for Human Arm Posture Prediction. 2012 World Congr Med Phys Biomed Eng 2012:1–4.

[24] Xie B, Zhao J. A new criterion for redundancy resolution of human arm in reaching tasks. 2013 IEEE/ASME Int Conf Adv Intell Mechatronics Mechatronics Hum Wellbeing, AIM 2013 2013:1066–71. https://doi.org/10.1109/AIM.2013.6584235.

[25] Jung ES, Choe J, Kim SH. Psychophysical cost function of joint movement for arm reach posture prediction. Proc Hum Factors Ergon Soc 1994;1:636–40.

[26] Zou Q, Zhang Q, Yang J (James), Gragg J. An inverse optimization approach for determining weights of joint displacement objective function for upper body kinematic. Robotica 2012:161–73. https://doi.org/10.1007/978-3-642-21799-9.

[27] Dumas R, Chèze L, Verriest J-P. Adjustments to McConville et al . and Young et al . body segment inertial parameters. J Biomech 2007;40:543–53.

[28] Olguín Díaz E. 3D Motion of Rigid Bodies. vol. 191. Springer; 2019.

[29] Grassia FS. Practical Parameterization of Rotations Using the Exponential Map. J Graph Tools 1998;3:29–48. https://doi.org/10.1080/10867651.1998.10487493.

[30] Engin AE, Chen SM. Statistical data base for the biomechanical properties of the human

shoulder complex II: Passive resistive properties beyond the shoulder complex sinus. J Biomech Eng 1986;108:222–7. https://doi.org/10.1115/1.3138606.

[31] Baerlocher P, Boulic R. PARAMETRIZATION AND RANGE OF MOTION OF THE BALL-AND-SOCKET JOINT. Deform Avatars 2001.

[32] Steel RGD, Torrie JH. Principles and Procedures of Statistics. (With special Reference to the Biological Sciences.). McGraw-Hill Book Company; 1960.

[33] Kiefer J. Sequential Minimax Search for a Maximum. Proc Am Math Soc 1953;4:502. https://doi.org/10.2307/2032161.

[34] Boulic R, Mas R, Thalmann D. Inverse Kinetics for Center of Mass Position Control and Posture Optimization. Image Process Broadcast Video Prod 1995.

[35] Riffard V, Chedmail P. Optimal Posture of a Human Operator and CAD in Robotics. 1996 IEEE Int. Conf. Robot. Autom., 1996, p. 1199–204.

[36] Rout B, Dash RR, Dhupal D. Optimization of Posture Analysis in Manual Assembly. Int J Mech Prod Eng Res Dev 2018;8:751–64.

[37] Lynn McAtamney, E. Nigel Corlett. RULA: a survey method for the investigation of work-related upper limb disorders. Applied Ergonomics, 1993, Vol. 24-2, p. 91-99, ISSN 0003-6870, https://doi.org/10.1016/0003-6870(93)90080-S.

[38] Chen, J., & Li, X. (2022). Determining human upper limb postures with a developed inverse kinematic method. *Robotica,* 1-23. doi:10.1017/S0263574722000789

[39] Chen, J. and Li, X. (2021), Development of a bi-criterion objective function for analytical inverse kinematic methods, in the proceedings of the 2021 CSME (Canadian Society of Mechanical Engineering) conference